

**Investigation of Protein Kinase D3 (PKD3) and ARGHAP11A (MP-GAP) Interaction: An  
Epitope Tag-based Co-Immunoprecipitation Approach**

By

Shamila Yazdanpanah

A thesis submitted to the

School of Graduate Studies

In partial fulfillment for the degree of

Master of Science in Medicine- Cancer and Development

Division of BioMedical Sciences

Faculty of Medicine

Memorial University

May 2025

St John's

Newfoundland and Labrador

## ABSTRACT

Protein interactions are fundamental to cellular signaling and regulatory pathways, driving diverse biological processes. This thesis investigates the potential interaction between protein kinase D3 (PKD3) and ARHGAP11A (MP-GAP) using an epitope tag-based co-immunoprecipitation approach. PKD3, a member of the protein kinase D family, is implicated in cell cycle regulation, cytokinesis, and cancer progression, while MP-GAP is a critical Rho GTPase-activating protein involved in cytokinesis. Given their roles, this study hypothesizes a functional relationship between PKD3 and MP-GAP in regulating cytokinesis via RhoA activity modulation.

To explore this interaction, a system was developed for the expression and detection of epitope-tagged PKD3 and MP-GAP in mammalian cells. Optimized protocols for cloning, protein expression, and immunoprecipitation were established. Despite validation of constructs and experimental conditions, co-immunoprecipitation experiments failed to confirm a direct interaction. Challenges such as low expression levels, nonspecific antibody binding, and potential transient or weak interactions were addressed.

These findings highlight the challenges inherent in studying transient or weak protein interactions, emphasizing the importance of leveraging complementary methods such as cross-linking or mass spectrometry to overcome experimental limitations. While no direct interaction was observed, this research provides insights into the complexities of PKD3's regulatory functions in cytokinesis. It sets the stage for future studies aimed at unraveling its broader role in cell cycle regulation and its potential as a therapeutic target in cancer biology.

## GENERAL SUMMARY

Proteins are the building blocks of life, working together to control essential processes like cell division, communication, and growth. This study focuses on two proteins, protein kinase D3 (PKD3) and ARHGAP11A (MP-GAP), and investigates whether they interact during cytokinesis—the final stage of cell division. PKD3 is important for regulating the cell cycle and is associated with cancer, while MP-GAP helps manage another protein, RhoA, which plays a key role in cytokinesis.

To explore their potential connection, a series of experiments were conducted using techniques designed to detect interactions between proteins. Although the experiments did not confirm a direct interaction, this could be due to challenges like low protein levels or interactions that happen too quickly to capture.

This research highlights the complexity of studying proteins and suggests that advanced tools could uncover more about these proteins' roles. Understanding how they work could eventually lead to finding more cancer treatment options.

## ACKNOWLEDGEMENTS

Completing this thesis has been a journey marked by both challenges and growth, and I am deeply grateful to those who supported me along the way. To my family and loved ones, thank you for being my steadfast pillars of encouragement, and offering unwavering support that carried me through this process. To my colleagues, your camaraderie, shared perseverance and humour have made an indelible mark on this journey, and I am deeply thankful for that.

I would also like to express my gratitude to my supervisor, Dr. Michael Leitges, for providing me with the opportunity to undertake this project. The experience has equipped me with invaluable lessons that I will carry forward. In addition, I would like to thank my committee members, Dr. Ann Dorward and Dr. Tom Belbin for their guidance, insightful feedback, and mentorship throughout this journey.

This work would not have been possible without the financial support provided by the Canadian Institutes of Health Research (CIHR), the School of Graduate Studies, and the Faculty of Medicine at Memorial University. Your contributions have allowed me to pursue this research and gain invaluable experiences.

Finally, this experience has taught me resilience, adaptability, and the importance of embracing both the highs and lows of scientific inquiry. These lessons have profoundly shaped my perspective, and I am thankful for the growth they have inspired.

# Table of Contents

<b>Chapter I- Introduction .....</b>	<b>1</b>
<b>1.1 Cellular Signaling and Protein Interactions.....</b>	<b>1</b>
<b>1.2 Protein Kinases as Key Regulators in Cellular Signaling .....</b>	<b>2</b>
<b>1.3 DAG Signalling and Protein Kinase C.....</b>	<b>2</b>
<b>1.4 Protein Kinase D Family .....</b>	<b>5</b>
1.4.1 A Brief Overview of Protein Kinase D Discovery.....	5
1.4.2 Isoform Structural Insights.....	7
1.4.3 Regulatory Mechanisms of Protein Kinase D Activity .....	10
1.4.3.1 The Canonical Activation Pathway .....	10
1.4.3.2 Subcellular Activation and Physiological Function .....	10
<b>1.5 Protein Kinase D3 .....</b>	<b>14</b>
<b>1.6 Cytokinesis and Protein Kinases .....</b>	<b>16</b>
1.6.1 RhoA Regulation .....	17
<b>1.7 Rationale and Objectives of the Predicted PKD3 and ARHGAP11A(MP-GAP) Interaction .</b>	<b>23</b>
<b>Chapter II- Materials and Methods .....</b>	<b>25</b>
<b>2.1 Cell Lines and Cell Culture.....</b>	<b>25</b>
2.1.1 Stable Cell Lines.....	25
<b>2.2 Plasmids and Constructs .....</b>	<b>26</b>
<b>2.3 Cloning.....</b>	<b>27</b>
2.3.1 Amplification of PKD3 and MP-GAP Sequences .....	27
2.3.2 TOPO TA Subcloning .....	29

2.3.3 Cloning into Mammalian Expression Vector containing GST Tag .....	29
2.3.4 Cloning into Lentiviral Production Vector for Establishing Stable Cell Lines .....	31
<b>2.3 Expression of epitope-tagged proteins .....</b>	<b>33</b>
2.3.1 Transfection .....	33
<b>2.4 Western Blotting .....</b>	<b>34</b>
2.4.1 Cell lysis, Protein Extraction, Protein Quantification .....	35
2.4.2 SDS-PAGE .....	36
2.4.3 Immunoblotting .....	37
2.4.4 Western Blot Imaging .....	37
<b>2.5 Immunoprecipitation .....</b>	<b>38</b>
<b><i>Chapter III-Results</i> .....</b>	<b>40</b>
<b>3. Results .....</b>	<b>40</b>
<b>3.1 Plasmid Cloning and Validations .....</b>	<b>40</b>
3.1.1 GST-fusion Constructs (pcDNA3.1-mPKD3-GST, pcDNA3.1-hMP-GAP-GST) .....	42
3.1.2 Lentiviral Constructs (psLenti-PKD3-FLAG, pLenti-MP-GAP-FLAG) .....	46
<b>3.2 Epitope-tagged protein transient expression .....</b>	<b>50</b>
3.2.1 Expression Discrepancy Between PKD3-FLAG and MP-GAP-FLAG in Transient Transfections .....	54
<b>3.3 Immunoprecipitation of PKD3-FLAG and MP-GAP-FLAG Optimization .....</b>	<b>59</b>
<b>3.4 Co-Immunoprecipitation .....</b>	<b>64</b>
3.4.1 Co-IP positive control: TRIM47-Myc and PKD3-FLAG .....	64
3.4.2 PKD3-FLAG and MP-GAP-HA Co-immunoprecipitation .....	67
<b><i>Chapter IV</i> .....</b>	<b>73</b>
<b>4. Discussion .....</b>	<b>73</b>
<b>4.1 Potential Causes for Experimental Setbacks .....</b>	<b>73</b>

4.1.1 Exploring the Lack of MP-GAP-GST Expression and Differential Expression of FLAG-Tagged Constructs .....	73
4.1.2 Background Noise and Antibody Binding .....	75
<b>4.2. Interpreting the Lack of Interaction in Co-IP: Implications and Future Directions .....</b>	<b>76</b>
4.2.1 Low Protein Expression as a Negative Impact on the Co-IP .....	77
4.2.2. Influence of Post-Translational Modifications and Subcellular Localization .....	78
4.2.3 Weak or Transient Interactions .....	79
4.2.4 Indirect Interactions and Complex Formation .....	80
<b>4.3 Studying PKD3 in the Context of the Cell Cycle and Cytokinesis.....</b>	<b>81</b>
4.3.1 Synchronization of Cells and Time-course Analysis for Improved Detection.....	82
<b>4.4 Future Directions .....</b>	<b>83</b>
<b>4.5 Implications for Cancer Research and Therapeutic Strategies .....</b>	<b>84</b>

## LIST OF FIGURES

Figure 1. Structural organization of PKC isoforms. ....	4
Figure 2. Domain Structure of PKD Family Members .....	9
Figure 3. Subcellular Roles and Activation of PKD in Response to Cellular Stimuli .....	13
Figure 4. Regulation of RhoA Activation and Deactivation by GEFs and GAPs .....	19
Figure 5. RhoA Regulation and Its Role in Cytokinesis .....	22
Figure 6. Cloning Strategy for Developing GST-Tagged and Lentiviral Constructs .....	41
Figure 7. Restriction Enzyme Validation of TOPO TA Subcloning Step in Cloning of GST Constructs..	44
Figure 8. GST Constructs Restriction Enzyme Validation .....	45
Figure 9. Restriction Enzyme Validation of TOPO TA Subcloning Step in Cloning of Lentiviral Constructs .....	48
Figure 10. Lentiviral Constructs Restriction Enzyme Digestion .....	49
Figure 11. Suboptimal Efficiency of Initial Transfection Experiments .....	51
Figure 12. Transfection Optimization in CHO-K1 and HEK293A Cell Lines .....	53
Figure 13. Western Blot Analysis of FLAG-tagged Protein Expression in HEK293A Cells Using the Optimized Transfection Protocol .....	55
Figure 14. Transient Expression of GST Constructs Developed In-house and Purchased HA Construct..	59
Figure 15. Comparison of Lysis Buffers for Immunoprecipitation Using Anti-DYKDDDDK Affinity Resin .....	62
Figure 16. MP-GAP-FLAG Immunoprecipitation.....	63
Figure 17. Successful Co-Immunoprecipitation of PKD3-FLAG and TRIM47-MYC as a Positive Control .....	66
Figure 18. PKD3-FLAG and MP-GAP-HA Co-Immunoprecipitation .....	68
Figure 19. Investigation of Nonspecific Bands Across Various Elution Methods in IP Experiments.....	71
Figure 20. Analyzing the Origin of the Non-specific Band .....	72

## LIST OF TABLES

Table 1. Primers Used for Fragment Amplification in GST and Lentiviral Construct Cloning .....	28
Table 2. PCR Parameters .....	28
Table 3. Restriction Enzymes used in Plasmid linearization and validation for GST vector constructs ....	31
Table 4. Restriction Enzymes used in Plasmid linearization and validation for Lentiviral vector constructs .....	32
Table 5. General Restriction Enzyme Digestion Setup.....	33
Table 6. Antibodies and dilutions used for immunoblotting.....	34
Table 7. Cell Lysis Buffer Composition .....	36

## LIST OF ABBREVIATIONS

APEX	Ascorbate peroxidase proximity labeling
ARHGAP11A	Rho GTPase-activating protein 11A
ATP	Adenosine Triphosphate
BamHI	Bacillus amyloliquefaciens restriction Enzyme H I
C-Jun	Cellular Jun
CAMKs	Calcium/calmodulin-dependent protein kinases
CBP	Calmodulin-binding peptide
CDKs	Cyclin-dependent kinases
cDNA	Complementary DNA
CHO-K1	Chinese hamster ovary-K1 cells
CMV	Cytomegalovirus
Co-IP	Co-Immunoprecipitation
COS-7	Cercopithecus aethiops kidney fibroblast-like cells
DAG	Diacylglycerol
DNA	Deoxyribonucleic acid
EcoRI	Escherichia coli restriction enzyme I
Ect2	Epithelial cell transforming sequence 2
EDTA	Ethylenediaminetetraacetic acid
ERK	Extracellular signal-regulated kinase
FLAG	Flagellin tag (DYKDDDDK)
GAPDH	Glyceraldehyde-3-phosphate dehydrogenase
GAPs	GTPase-activating proteins
GDP	Guanosine diphosphate
GEFs	Guanine nucleotide exchange factors
GFP	Green fluorescent protein
GID4	Glucose-induced degradation protein 4 homolog Complex Subunit 4
E3	E3 ubiquitin-protein ligase
GIT1	G protein-coupled receptor kinase interacting protein 1
GPCRs	G protein-coupled receptors
GST	Glutathione S-Transferase
GTP	Guanosine triphosphate
HA	Hemagglutinin
HDAC	Histone deacetylase
HEK293	Human embryonic kidney 293 cells
hGID	Human Glucose-induced degradation complex
HindIII	Haemophilus influenzae restriction enzyme III
HRP	Horseradish peroxidase
IKK $\beta$	Inhibitory kappa B kinase beta
IL-6	Interleukin 6
IP3	Inositol trisphosphate
I $\kappa$ B $\alpha$	Nuclear factor-kappa B inhibitor alpha

MEF	Mouse embryonic fibroblasts
MEK	Mitogen-activated protein kinase
MgcRacGAP	Male germ cell Rac GTPase-activating protein
MMPs	Matrix metalloproteinases
MnSOD	Manganese-dependent superoxide dismutase
MS	Mass spectrometry
MUNC13	Mammalian uncoordinated-13
Myc	Myelocytomatosis viral oncogene
NF $\kappa$ B	Nuclear factor kappa B
NotI	Nocardia otitidis restriction enzyme I
NP-40	Nonidet P-40
PAK4	p21-activated kinase 4
PCR	Polymerase chain reaction
PDK1	Phosphoinositide-dependent protein kinase-1
PDZ	Postsynaptic density 95/discs large/Zonula Occludens
PFI-7	Small molecule inhibitor of SETD7
PH	Pleckstrin homology
PIP2	Phosphatidylinositol 4,5-bisphosphate
PKA	Protein Kinase A
PKB	Protein Kinase B
PKC	Protein Kinase C
PKC $\epsilon$	Protein Kinase C Epsilon
PLC	Phospholipase C
PLKs	Polo-like kinases
PS	Phosphatidylserine
PstI	Providencia stuartii restriction enzyme I
PuroR	Puromycin resistance
PvuI	Proteus vulgaris restriction enzyme I
Raf	Rapidly accelerated fibrosarcoma kinase
Ras	Rat Sarcoma virus oncogene
RasGRPs	Ras guanyl nucleotide releasing proteins
RhoA	Ras homolog family member A
RIN1	Ras and Rab interactor 1
ROS	Reactive oxygen species
RSK	Ribosomal S6 Kinase
RTKs	Receptor tyrosine kinases
Scal	Streptomyces caespitosus Restriction Enzyme I
SDS-PAGE	Sodium Dodecyl Sulfate-Polyacrylamide Gel Electrophoresis
Ser	Serine
SSH1L	Slingshot homolog1
StuI	Streptomyces tubercidicus Restriction Enzyme I
sulfo-SBED	Sulfosuccinimidyl-2-[6-(biotinamido)-2-(p-azidobenzamido)-hexanoamido]ethyl-1,3'-dithiopropionate

TAP	Tandem affinity purification
TBST	Tris-buffered saline with Tween-20
TGN	Trans-Golgi Network
Thr	Threonine
TRIM47	Tripartite motif containing 47
ULD	Ubiquitin-like domain
VEGF	Vascular endothelial growth factor
WRPE	Woodchuck hepatitis virus post-transcriptional regulatory element
XcmI	Xanthomonas campestris Restriction Enzyme I

## **Chapter I- Introduction**

### **1.1 Cellular Signaling and Protein Interactions**

Proteins are key to signaling processes coordinating the cellular functions of living organisms. Signal transduction involves protein-mediated processes that can be represented, for example, by cell surface receptors that are activated by the binding of ligands, thereby transmitting signals to effector proteins through second messengers, ultimately leading to a specific cellular response. Within this framework, proteins carry out distinct roles, including catalyzers, modulators, and sensors. Catalyzers, such as enzymes like kinases, transmit signals by catalyzing specific post-translational modifications on target proteins. Conversely, modulators like phosphatases regulate signal intensity by removing these modifications. Sensors, on the other hand, recognize and respond to these modifications. They facilitate protein-protein interactions or directly bind to specific molecules, thereby modulating signal transduction pathways.

These proteins operate on short amino acid sequences, called motifs, encoding cellular signals. Through their coordinated action, cells efficiently transduce external cues and ensure accurate signal transduction. Protein level, localization, activity, and interaction variations are crucial for precise signal transduction. They enable cells to respond to diverse cues and adjust their responses' sensitivity, duration, and dynamics. <sup>1</sup>

## **1.2 Protein Kinases as Key Regulators in Cellular Signaling**

Protein phosphorylation is a reversible process carried out by protein kinases which involves adding a phosphate group to the polar group R of different amino acids. This process plays a crucial regulatory role in several cellular functions, including protein synthesis, cell division, signal transduction, growth, development, and aging. <sup>2</sup>

Protein kinases catalyze the transfer of the  $\gamma$ -phosphate group from Adenosine Triphosphate (or occasionally Guanosine Triphosphate) to specific amino acid residues on their target proteins. The most common phosphorylation sites in eukaryotic cells are serine, threonine, and tyrosine residues, although histidine can also be phosphorylated. The addition of a phosphate group can significantly alter the protein's function by inducing conformational changes or by creating or disrupting protein-protein interaction surfaces. These modifications can activate or deactivate enzymes, modulate protein-protein interactions, alter subcellular localization, or mark proteins for degradation.<sup>3</sup> The versatility of phosphorylation as a regulatory mechanism is evident in the fact that approximately 30% of cellular proteins are phosphorylated by kinases, despite kinase genes constituting only about 2% of eukaryotic genomes. <sup>4</sup>

## **1.3 DAG Signalling and Protein Kinase C**

Diacylglycerol (DAG), a lipid second messenger, serves as a key mediator in transducing extracellular signals to intracellular effectors, thereby regulating many physiological functions. The DAG pathway is initiated by activating cell surface receptors, such as G protein-coupled receptors (GPCRs) or receptor tyrosine kinases (RTKs), in response to extracellular stimuli such as hormones, growth factors, or neurotransmitters. Upon receptor activation, phospholipase C

(PLC) is activated <sup>5</sup> and catalyzes the hydrolysis of phosphatidylinositol 4,5-bisphosphate (PIP<sub>2</sub>) into two secondary messengers: inositol 1,4,5-trisphosphate (IP<sub>3</sub>) and DAG <sup>5</sup>. It is of particular interest that DAG serves as a critical signaling molecule, exerting its effects through various downstream effectors. One of the primary targets of DAG is the Protein Kinase C (PKC) family<sup>6</sup>, a group of serine/threonine (Ser/Thr) kinases. Activated PKC modulates the activity of numerous intracellular proteins, including enzymes, ion channels, and transcription factors, thereby regulating a variety of cellular processes such as cell proliferation, differentiation, apoptosis, and metabolism .

The discovery of PKC in the 1970s by Yasutomi Nishizuka and colleagues, was a landmark achievement in understanding cellular signaling mechanisms, especially by Ser/Thr kinases. PKCs were identified as a novel class of protein kinases activated by calcium ions and DAG <sup>6,7</sup>, distinguishing them from previously known kinases such as Protein Kinase A (PKA)<sup>8</sup>. PKC isoforms are classified according to their structural and activation properties. There are nine PKC genes that code for different PKC isoforms that are grouped into three categories: classical or conventional PKCs (cPKCs; PKC $\alpha$ , PKC $\beta$ I, PKC $\beta$ II, and PKC $\gamma$ ) are calcium-dependent and activated by both phosphatidylserine (PS) and DAG; novel PKCs (nPKCs; PKC $\delta$ , PKC $\epsilon$ , PKC $\eta$ , and PKC $\theta$ ) which are calcium-independent and regulated by DAG and PS; and atypical PKCs (aPKCs; PKC $\zeta$  and PKC $\lambda$ ) are calcium-independent and activated without DAG, though PS can modulate their activity. <sup>9</sup> Figure 1 provides a detailed schematic overview of the PKC family, highlighting each individual structural component and its organization within the protein family.

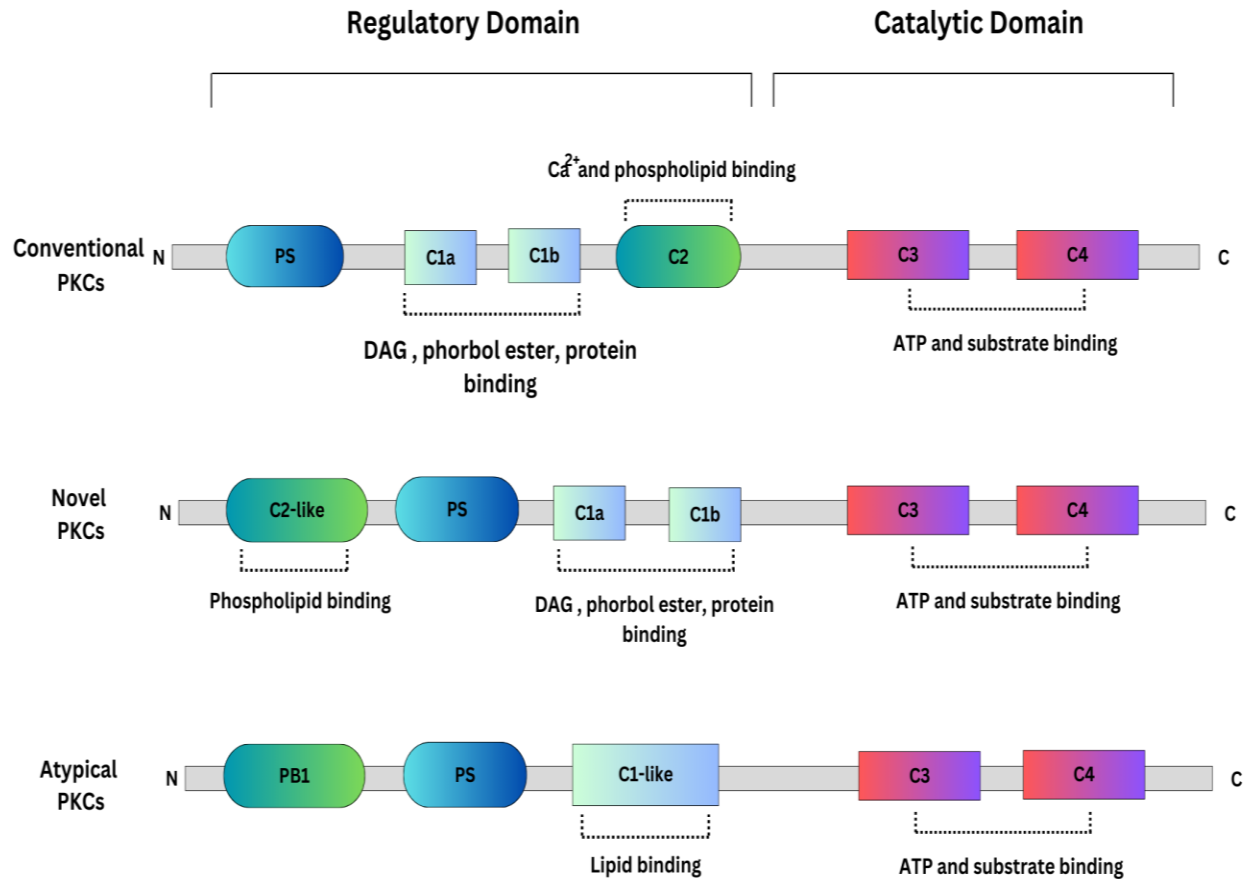


**Figure 1. Structural organization of PKC isoforms.**

Conventional PKCs are characterized by a regulatory domain containing a C2 domain (involved in calcium and phospholipid binding) and two C1 domains (C1a and C1b) that bind diacylglycerol (DAG), phorbol esters, and proteins. The catalytic domain consists of the C3 and C4 regions, responsible for ATP and substrate binding. Novel PKCs lack the C2 domain, making them calcium-independent, but still possess the C1 domains and a similar catalytic domain. Atypical PKCs are distinct in lacking the conventional C1 and C2 domains, instead having a PB1 domain and a C1-like domain that does not bind DAG or phorbol esters. Despite structural differences, all PKCs share the common C3 and C4 catalytic regions required for kinase activity. Activation requirements vary across classes: cPKCs require calcium, DAG, and phosphatidylserine (PS), nPKCs require DAG and PS but are calcium-independent, and aPKCs are activated independently of calcium and DAG, although PS can modulate their activity.

(Adapted from: He, S.; Li, Q.; Huang, Q.; Cheng, J. Targeting Protein Kinase C for Cancer Therapy. *Cancers* **2022**, *14*,1104. <https://doi.org/10.3390/cancers14051104> . Reproduced under Creative Commons Attribution (CC BY) license (<https://creativecommons.org/licenses/by/4.0/>).

In addition to PKCs, five other distinct DAG receptors have been identified in cells: protein kinase D family, Chimaerins that belong to Rac GTPase-activating proteins (RacGAPs) family, Ras guanyl nucleotide-releasing proteins (RasGRP), Mammalian Uncoordinated-13 (MUNC13) scaffolding proteins, and Diacylglycerol kinase (DAGK) family. While the PKD family plays a crucial role in transducing DAG-mediated signals into cellular responses, Chimaerins regulate the activity of small GTPases, thereby influencing cytoskeletal dynamics and cell migration.<sup>10-12</sup> RasGRP acts as a crucial modulator of Ras and Rap1 signaling pathways, controlling cell proliferation and differentiation.<sup>13,14</sup> MUNC13 scaffolding proteins are indispensable for the organization of signaling complexes involved in synaptic vesicle priming.<sup>15</sup> Lastly, DAG kinases regulate DAG levels by converting DAG into phosphatidic acid, thus modulating lipid signaling and membrane dynamics.<sup>16</sup> Similarly, all these molecules contain C1 domains, which facilitate their interaction with DAG and regulate downstream signaling events in a phospholipid-dependent manner analogous to that observed with PKCs.

The PKC-PKD signaling axis significantly amplifies DAG-initiated signaling by facilitating PKD-mediated phosphorylation of diverse substrates, which allows for a broader range of cellular responses. Additionally, activated PKD is capable of translocating to various cellular compartments, including the nucleus, the Golgi apparatus, and mitochondria.<sup>17</sup> This extends the influence of DAG signaling. The activation of PKD can persist longer than the initial DAG stimulus, providing a mechanism for sustained signaling responses.<sup>18</sup>

## **1.4 Protein Kinase D Family**

### **1.4.1 A Brief Overview of Protein Kinase D Discovery**

The story of protein kinase D discovery begins with the discovery of the first family member, protein kinase D1 (PKD1), in 1994, when Johannes et al. screened a mouse cDNA library for PKC-related kinases followed by the subsequent characterization of PKD3 in 1999 , and PKD2 in 2001.<sup>19-21</sup> PKD family members were initially classified as a new members of the PKCs, due to their high structural similarity. This structural resemblance, coupled with the presence of a DAG-binding C1 domain, led to the preliminary classification of PKD1 as an atypical PKC, designated as PKC $\mu$  for human PKD1 and PKC $\nu$  for PKD3. However, further investigation revealed substantial structural homology between PKD's catalytic domain and the Ca<sup>2+</sup>/calmodulin-dependent protein kinases (CAMKs), which consequently lead to a re-classification of PKD into the CAMK group.<sup>22</sup>

The extent of research and understanding varies significantly among the different PKD isoforms. PKD3 remains relatively less studied when compared to PKD1 and PKD2. Most of the available literature and experimental data concentrate on PKD1, providing more detailed insights into its activation mechanisms and regulatory pathways. This disparity in research attention has resulted in significant gaps in our understanding of PKD3, particularly concerning its specific functions and regulatory controls. In the following sections of this introduction, the term “PKD” will primarily refer to PKD1, given the abundance of information available about this isoform. By reference to the well-documented characteristics of PKD1, the aim is to highlight the current knowledge landscape and emphasize the need for further investigation into PKD3. This comparative approach will help elucidate the unique and potentially critical roles that PKD3 may play in cellular signaling and regulation.

## 1.4.2 Isoform Structural Insights

The PKD family, comprising the PKD1, PKD2, and PKD3 isoforms, exhibits high conservation across evolutionary time. Each isoform consists of 912, 878, and 890 amino acids (aa), respectively for human PKD1, PKD2, and PKD3. PKD1 and PKD2 share a high degree of similarity in their domain architecture, with approximately 85-90% sequence identity and conserved structural elements (as shown in Figure 2). This includes similarities in key functional domains such as the kinase domain, regulatory motifs, and other structural features that contribute to their homologous functions.<sup>23</sup> The conserved structure of PKD comprises an N-terminal regulatory region containing a C1 domain and a pleckstrin homology (PH) domain, followed by a C-terminal catalytic domain. The C1 domain contains two cysteine-rich Zn-finger-like motifs, C1a and C1b, which bind DAG and phorbol esters, thereby facilitating PKD's localization to various cellular compartments.<sup>24</sup> The PH domain has been demonstrated to play an autoinhibitory role in maintaining kinase inactivity under basal conditions.<sup>25</sup> More recent findings have also identified a ubiquitin-like domain (ULD) shared among all three PKD isoforms, located at the N-terminus. It is proposed that the ULD may initiate PKD dimerization at the membrane, thereby facilitating trans-autophosphorylation and subsequent activation in response to increased DAG levels, potentially independently of PKC.<sup>26,27</sup> In addition to the regulatory regions, PKD1 and PKD2 also feature a C-terminal PDZ-binding motif, which enables interactions with other PDZ domain-containing proteins, thereby potentially influencing their localization and function. This motif includes autophosphorylation sites (S910 in PKD1 and S876 in PKD2) that can serve as markers for PKD activation status and may have further functional roles.<sup>28</sup> The C-terminal catalytic domain of PKD is highly conserved across all isoforms, containing several key residues that are necessary for kinase activity. These include

autophosphorylation sites such as S738 and S742 in PKD1, S706 and S710 in PKD2, and S731 and S735 in PKD3, which are critical for the enzymatic activity and regulation of PKD.<sup>29</sup>A schematic representation of the PKC family including the individual structural components is shown in Figure 2.

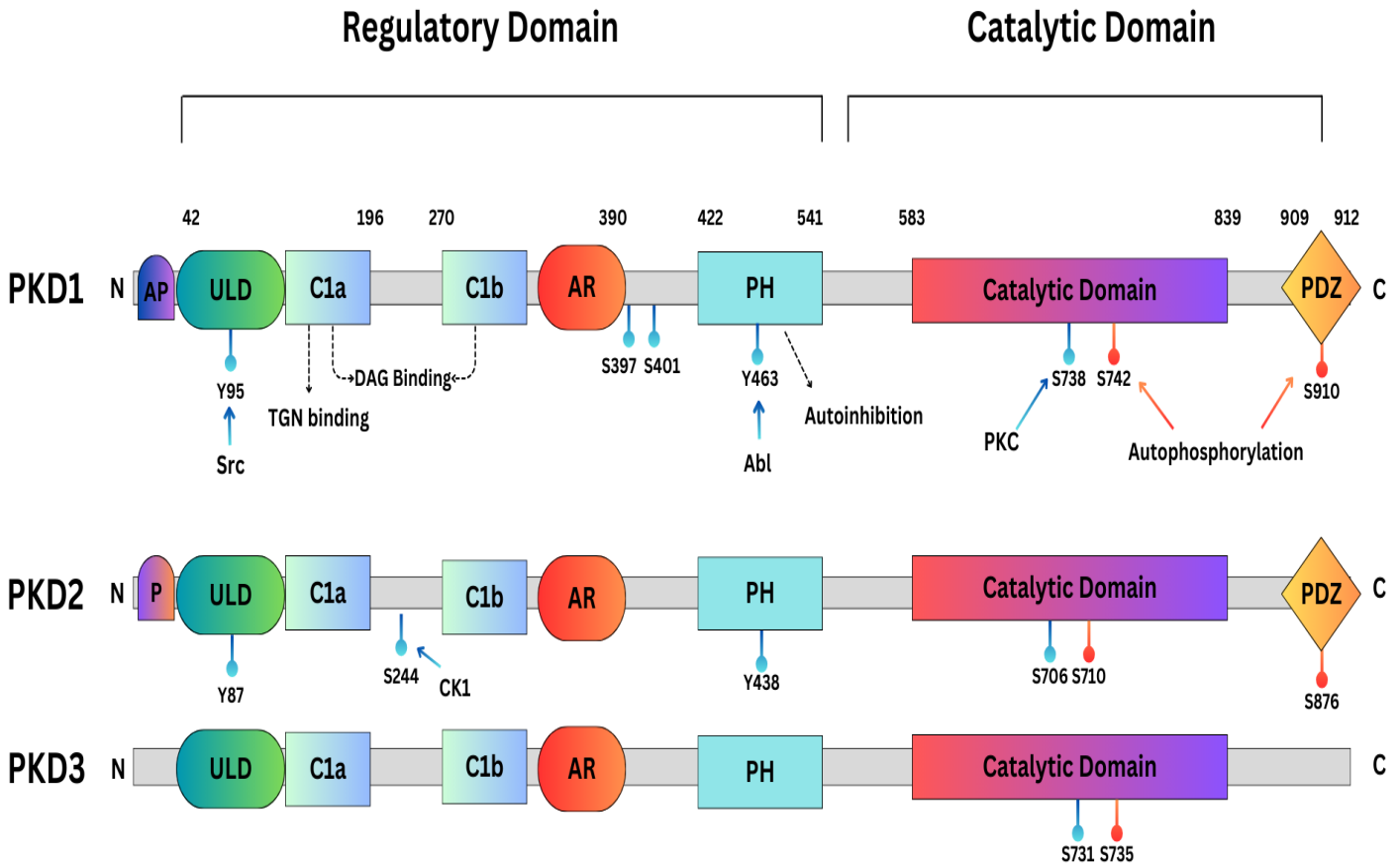


**Figure 2. Domain Structure of PKD Family Members**

The figure illustrates the structural organization of the three protein kinase D (PKD) isoforms in human: PKD1, PKD2, and PKD3. Each isoform features an N-terminal regulatory domain and a C-terminal catalytic domain. The regulatory domain includes a Ubiquitin-like Domain (ULD), two cysteine-rich domains (C1a and C1b) involved in diacylglycerol (DAG) binding and membrane localization, an Autoinhibitory Region (AR), and a Pleckstrin Homology (PH) domain responsible for maintaining kinase inactivity. Other domains with less known functions are an alanine–proline-rich region (AP) for PKD1 and a proline-rich region (P) for PKD2. The C-terminal catalytic domain is essential for kinase activity, with specific autophosphorylation sites indicated for each isoform (S738, S742 in PKD1; S706, S710 in PKD2; S731, S735 in PKD3). PKD1 and PKD2 also have a PDZ-binding motif, facilitating protein interactions. Key phosphorylation sites involved in activation and regulatory interactions are highlighted for each isoform.

(Adapted from: Zhang, X.; Connelly, J.; Chao, Y.; Wang, Q.J. *Multifaceted Functions of Protein Kinase D in Pathological Processes and Human Diseases. Biomolecules* 2021, 11, 483. <https://doi.org/10.3390/biom11030483>. Reproduced under Creative Commons Attribution (CC BY) license (<https://creativecommons.org/licenses/by/4.0/>).

### 1.4.3 Regulatory Mechanisms of Protein Kinase D Activity

#### 1.4.3.1 The Canonical Activation Pathway

Upon receptor stimulation, PLCs hydrolyze PIP<sub>2</sub> to generate IP<sub>3</sub> and DAG. IP<sub>3</sub> promotes the release of calcium ions from the endoplasmic reticulum into the cytoplasm. DAG, along with calcium, binds to and holds PKC on the plasma membrane, initiating both their activation. In parallel, cytosolic PKD is recruited to the plasma membrane by DAG binding through its C1 domain. This process induces a conformational change, allowing PKC to colocalize with PKD and transphosphorylate specific serine residues in PKD's activation loop (Ser738 for PKD1, Ser706 for PKD2, Ser731 for PKD3.) Following the initial phosphorylation by PKC, PKD autophosphorylates the adjacent serine residue (Ser742 for PKD1, Ser710 for PKD2, Ser735 for PKD3). The phosphorylation events lead to the relief of autoinhibition by the PH domain, resulting in full activation of PKD.<sup>30</sup>

#### 1.4.3.2 Subcellular Activation and Physiological Function

PKD can be activated at multiple subcellular locations, each associated with distinct physiological functions. PKD has been identified as a trans-Golgi network resident enzyme<sup>31</sup>, and evidence suggests that it plays a role in regulating vesicle trafficking from the TGN to the cell surface. At the TGN, DAG-mediated recruitment of PKD facilitates its function in the regulation of vesicle trafficking, which is crucial for processes such as insulin secretion from pancreatic  $\beta$  cells.<sup>32,33</sup> Also, in vesicle trafficking and secretion, PKD regulates Golgi function and secretion by phosphorylating substrates like PI4KIIIb<sup>34</sup>. This is crucial for the fission of

trans-Golgi network transport carriers. The role of PKD in regulating cargo within the Golgi apparatus impacts cell motility, vesicle trafficking, and the recruitment of integrins to focal adhesions.<sup>34</sup>

Furthermore, the activation of PKD1 by growth-promoting G-protein-coupled receptor (GPCR) agonists has been observed to stimulate mitogenic signaling pathways, particularly in fibroblasts and cancer cells. In this context, PKD1 has been shown to enhance the duration of the mitogen-activated protein kinase kinase/extracellular signal-regulated kinase/ribosomal S6 kinase (MEK/ERK/RSK) pathway, thereby promoting cell cycle progression<sup>35-37</sup>. This is achieved through phosphorylation of Ras and Rab interactor 1 (RIN1), which facilitates Ras/Raf interaction and ERK activation, both of which are crucial for cell proliferation.

In another example in endothelial cells, it has been demonstrated that PKD signaling plays a pivotal role in Vascular Endothelial Growth Factor (VEGF)-induced processes, including ERK activation, gene expression, and Deoxyribonucleic Acid (DNA) synthesis (as evidenced by increased incorporation of [<sup>3</sup>H]thymidine, a marker of active DNA replication, confirming enhanced cell proliferation).

These processes are essential for the development of new blood vessels, a process known as angiogenesis.<sup>38</sup> Furthermore, Chang et al. (2008) demonstrated that PKD phosphorylates class II histone deacetylases (HDACs), causing their cytoplasmic retention and enabling the activation of VEGF-responsive genes, thereby promoting angiogenesis.<sup>39</sup>

Following its translocation to the plasma membrane and subsequent activation, PKD is capable of shuttling in and out of the nucleus, thereby regulating transcription factors such as Myocyte Enhancer Factor 2 (MEF2)<sup>40</sup>. The nuclear localization of PKD is regulated by various regions

within its domain structure, with different isoforms exhibiting unique regulatory mechanisms. PKD1 and PKD2 primarily exist in the cytoplasm but can translocate to the nucleus in response to specific stimuli, such as oxidative stress. In contrast, PKD3 shuttles between the nucleus and cytoplasm continuously.<sup>41</sup> In particular, oxidative stress exerts a significant influence on PKD signaling, particularly in the context of mitochondria-to-nucleus communication. The Storz group demonstrated that reactive oxygen species (ROS) activate PKD, thereby inducing the expression of antioxidative genes through NF $\kappa$ B activation<sup>42</sup>. The activation of PKD at the mitochondria is mediated by the tyrosine kinases c-Abl and Src, which phosphorylate PKD at specific tyrosine residues, thereby creating a docking site for protein kinase C delta (PKC $\delta$ ).<sup>14</sup> This interaction leads to the phosphorylation of PKD's activation loop by PKC $\delta$ , triggering its activation. Once activated, PKD phosphorylates IKK $\beta$ , which promotes the degradation of I $\kappa$ B $\alpha$  and subsequently activates NF $\kappa$ B.<sup>17</sup> In the nucleus, NF $\kappa$ B enhances the transcription of the *SOD2* gene, which encodes manganese-dependent superoxide dismutase. This protein detoxifies ROS and promotes cell survival.<sup>43</sup> A summary of PKD's role in cellular processes is presented in Figure 3.

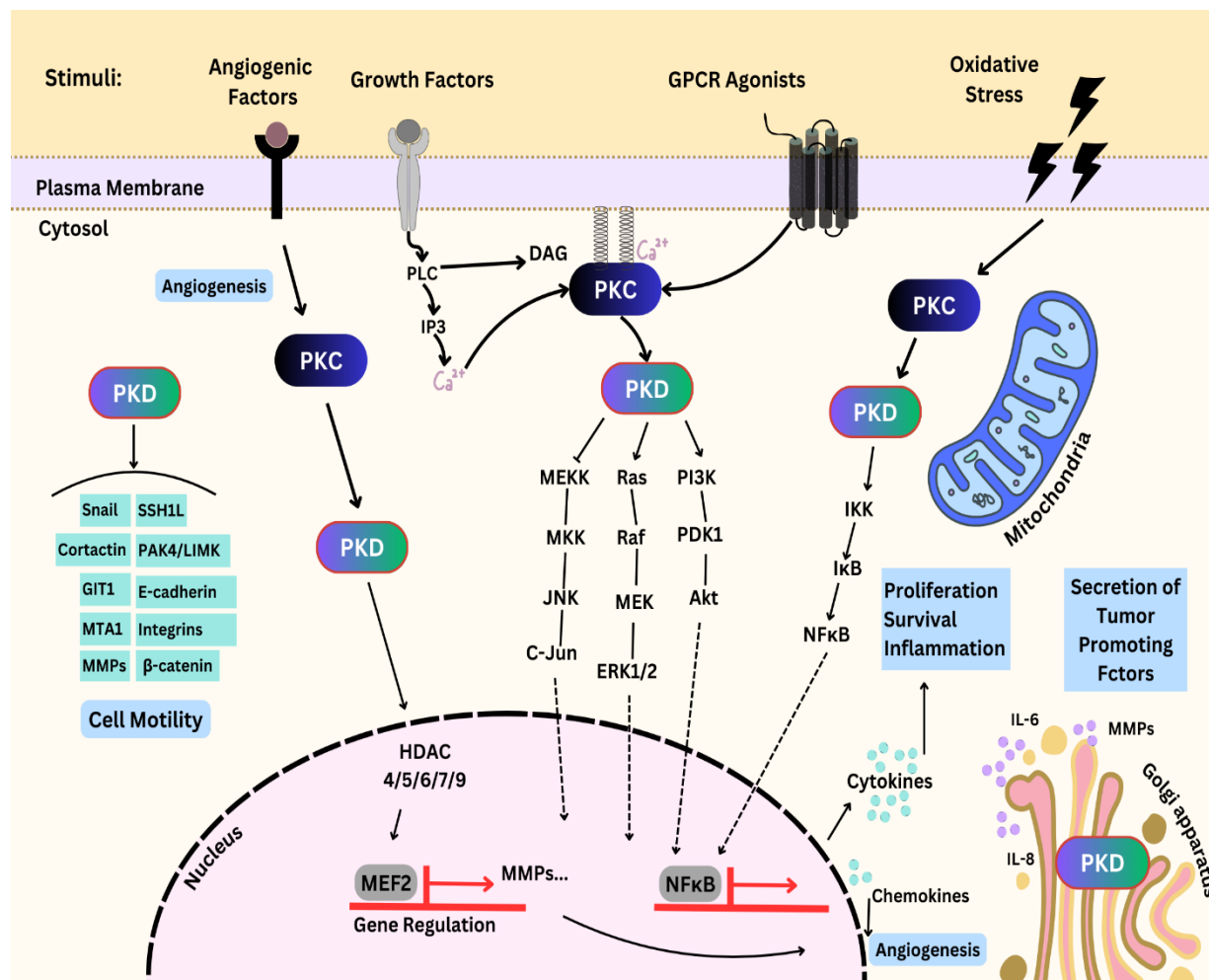


**Figure 3. Subcellular Roles and Activation of PKD in Response to Cellular Stimuli**

The figure illustrates the subcellular localization, activation, and physiological functions of PKD isoforms in response to various cellular stimuli, including angiogenic factors, growth factors, GPCR agonists, and oxidative stress, demonstrating its broad impact on cellular physiology. PKD is activated at multiple cellular sites, such as the plasma membrane, mitochondria, and Golgi apparatus, depending on the stimulus. At the plasma membrane, PKD is activated by diacylglycerol (DAG) and plays roles in signaling pathways involving MEK/ERK, NFκB, and JNK, which regulate gene expression, cell proliferation, survival, inflammation, and angiogenesis. PKD also translocates to the nucleus to modulate transcription factors like MEF2 and NFκB, influencing gene regulation and cellular responses to stress. In the mitochondria, PKD activation is linked to oxidative stress response, promoting antioxidant gene expression.

(Adapted from: Zhang, X.; Connelly, J.; Chao, Y.; Wang, Q.J. *Multifaceted Functions of Protein Kinase D in Pathological Processes and Human Diseases*. *Biomolecules* 2021, 11, 483. <https://doi.org/10.3390/biom11030483>. Reproduced under Creative Commons Attribution (CC BY) license (<https://creativecommons.org/licenses/by/4.0/>).

## 1.5 Protein Kinase D3

PKD3 displays distinctive structural characteristics that may underpin its functional distinction when compared to PKD1 and PKD2. A noteworthy distinction, as illustrated in Figure 2, is the absence of a C-terminal PDZ binding motif in PKD3. The C-terminal PDZ binding motif, which is present in PKD1 and PKD2, enables these proteins to regulate the localization and trafficking of specific target proteins, such as Kinase D-Interacting Substrate of 220 kDa (Kidins220). This is a crucial protein involved in neural cell surface dynamics and trafficking between the plasma membrane and the trans-Golgi network.<sup>44</sup> Another key structural difference is the absence of an autophosphorylation site at PKD3's C-terminus and the presence of an alanine- and proline-rich region at its N-terminus. In addition to these structural differences, PKD3 also displays distinctive localization patterns in comparison to PKD1 and PKD2. While PKD1 is primarily located within the cytosol under basal conditions<sup>45</sup>, it redistributes to various cellular compartments, including the Golgi apparatus, the nucleus, and mitochondria upon stimulation. Similarly, PKD2 is predominantly localized to the cytoplasm in unstimulated cells<sup>46</sup>. In contrast, PKD3 displays a distinct localization pattern, being present in both the cytoplasm and nucleus even in the absence of external stimuli<sup>47</sup>. The differential localization of PKD3 indicates that it is subject to unique spatial regulation within the cell in comparison to PKD1 and PKD2. This suggests that there may be differences in the cellular functions and signaling pathways associated with these proteins.

The research conducted thus far on PKD3 has considerably enhanced our comprehension of its function in diverse biological processes, with a particular emphasis on its implications in cancer progression and immune system regulation. Investigations have indicated that PKD3 plays a role in the promotion of cancer cell proliferation, growth, migration, and invasion across a range of

tumor types, including colorectal, gastric, hepatic, prostate, and breast cancer<sup>48</sup>. The findings indicate that PKD3 functions as an upstream regulator of pivotal signaling pathways implicated in cancer cell proliferation, such as the ERK1/c-MYC axis in breast cancer<sup>49</sup>. In another study<sup>50</sup>, also focusing on breast cancer, PKD3 has been identified as a downstream effector of Tripartite Motif Containing 47 (TRIM47) in the activation of NF- $\kappa$ B signaling. The results of this research indicate that the knockdown of PKD3 leads to a suppression of the proliferation of breast cancer cells, which suggests that PKD3 has growth-promoting effects. Furthermore, the reduction in PKD3 expression results in a decrease in the phosphorylation of IKK- $\alpha$  and IKK- $\beta$ , which suggests that PKD3 plays a role in the activation of NF- $\kappa$ B signaling in breast cancer cells. This signaling pathway is essential for cell survival and proliferation, and its activation by TRIM47 through the stabilization of PKD3 contributes to the resistance of breast cancer cells to endocrine therapies.<sup>50</sup>

The studies conducted in our group, which employed mouse embryonic fibroblast (MEF) cells depleted of PKD3, identified PKD3 as a modulator of microtubule dynamics during mitosis.<sup>51</sup> This provided insights into a unique PKD3 signaling pathway that was previously unknown. It was shown that PKD3 exhibits distinct subcellular localizations at different stages of cell cycle in MEFs. Under normal growth conditions, PKD3 exhibits a ubiquitous localization pattern, including within the nucleus. However, during prophase, the ubiquitous pattern changes, with PKD3 becoming specifically localized to centrosome structures.<sup>51</sup> This localization persists into metaphase, extending to the spindle structures, including the two centrosomes. The *in vitro* analysis of immortalized PKD3-deficient MEFs initially demonstrated alterations in the cell cycle, affecting microtubule dynamics. Also, the proliferation rate of PKD3-deficient MEFs was reduced, indicating that PKD3 plays a crucial role in cell cycle progression. Treatment with

nocodazole, which blocks microtubule polymerization, significantly impaired the proliferative capacity of PKD3-deficient MEFs following release, indicating a reduced ability to resume cell division. This indicates a mechanistic problem during microtubule polymerization in the absence of PKD3.<sup>51</sup> Moreover, preliminary data from Zhang et al. showed a binucleated phenotype in PKD3-deficient MEFs, indicating the failure of cytokinesis and emphasizing a previously unrecognized role for PKD3 in cell cycle regulation (unpublished data by Zhang et al.). These findings provide new insights into the intricate regulatory mechanisms that govern cell division and offer potential avenues for further research into the molecular basis of cell cycle regulation.

## **1.6 Cytokinesis and Protein Kinases**

The final stage of cell division, cytokinesis, is a highly regulated process that ensures the correct final separation of two daughter cells. This is achieved by, among other things, ensuring the equal partitioning of cytoplasmic contents between the two daughter cells. This process is of critical importance for the maintenance of genomic stability and is governed by a complex network of proteins, including kinases, which play a pivotal role in the precise orchestration of cytokinesis.

PKC $\epsilon$  has been established as a critical regulator of cytokinesis, orchestrating essential processes such as cleavage furrow formation and ingression. Research led by Peter Parker's group revealed that PKC $\epsilon$  is dynamically localized to the cleavage furrow during cytokinesis, suggesting its pivotal role in the spatial and temporal regulation of contractile ring assembly and contraction.<sup>52</sup> During the late stages of mitosis, PKC $\epsilon$  interacts with 14-3-3 proteins via its V3 region, forming a complex essential for successful abscission. Mutation of the V3 phosphorylation sites disrupts this interaction, impairing cytokinesis completion. Similarly, knockout, depletion, or

pharmacological inhibition of PKC $\epsilon$  hampers abscission.<sup>52,53</sup> The mechanism by which PKC $\epsilon$  facilitates abscission is not fully understood but may involve the small GTPase RhoA. PKC $\epsilon$  inhibition is associated with prolonged RhoA activation and its persistent localization at the actomyosin ring<sup>52</sup>, which contracts to form the cleavage furrow. While the substrates phosphorylated by PKC $\epsilon$  to regulate RhoA activity remain unidentified, potential candidates include RhoA guanine nucleotide exchange factors or GTPase-activating proteins.<sup>52,53</sup>

The relationship between PKC and PKD in the context of cell cycle regulation is complex and interconnected. Given that PKC $\epsilon$  has been demonstrated to activate PKD3<sup>54</sup>, these findings in conjunction with similar phenotypes observed in PKC $\epsilon$  and PKD3-deficient MEFs (unpublished data by Zhang et al.) indicate the existence of a functional link between PKC $\epsilon$  and PKD3 in the regulation of cytokinesis. Based on these data, it is proposed that PKC $\epsilon$ , by activating PKD3, could coordinate the regulation of both microtubule dynamics and actin cytoskeleton reorganization, thereby ensuring proper cleavage furrow formation and successful cell division.

### 1.6.1 RhoA Regulation

The interplay between guanine nucleotide exchange factors (GEFs), RhoA, and GTPase-activating proteins (GAPs) is crucial for the precise regulation of cytokinesis. RhoA plays a pivotal role in orchestrating the assembly and contraction of the actomyosin ring at the cleavage furrow. The spatiotemporal activation of RhoA, as shown in Figure 4, is subject to strict regulation by GEFs, which facilitate the exchange of GDP for GTP, thereby activating RhoA, and GAPs, which accelerate the hydrolysis of GTP to GDP, thereby deactivating RhoA. This regulatory cycle is of great importance in ensuring that RhoA is activated at the appropriate time

and location during cytokinesis and enables the formation of the contractile ring and its subsequent contraction, which drives the ingression of the cleavage furrow and completes the process of cell division.<sup>55</sup>

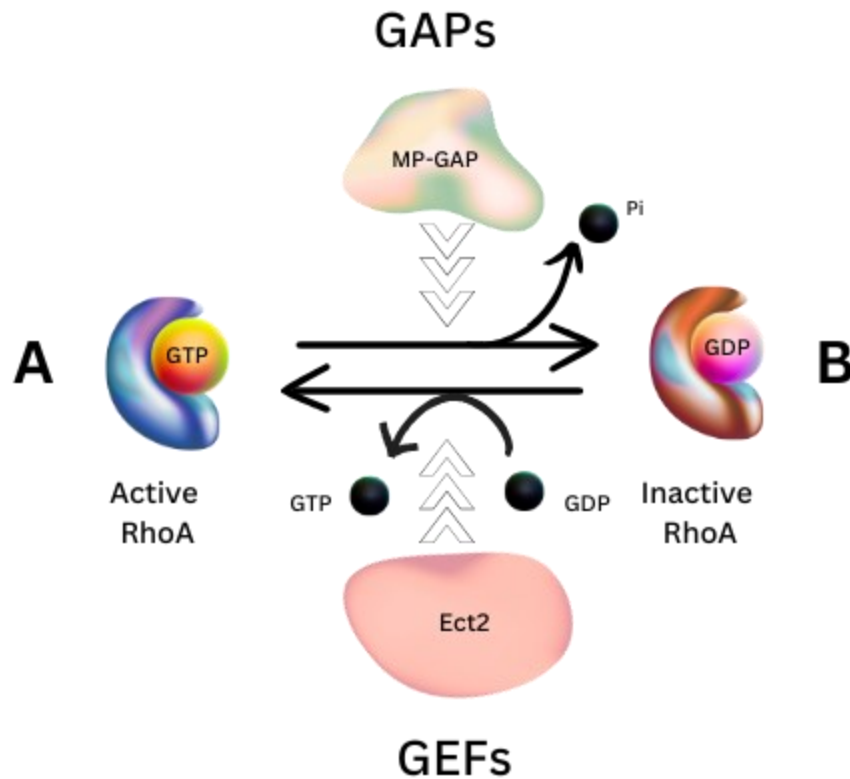


**Figure 4. Regulation of RhoA Activation and Deactivation by GEFs and GAPs**

This figure illustrates the regulation of RhoA, a small GTPase, between its active (RhoA-GTP, A) and inactive (RhoA-GDP, B) states. GEFs, such as Ect2, facilitate the activation of RhoA by promoting the exchange of GDP for GTP, transitioning it to its active state (A). In contrast, GAPs, such as MP-GAP, catalyze the hydrolysis of GTP to GDP, converting RhoA back to its inactive state (B). This tightly regulated cycle is crucial for processes such as cytokinesis and actomyosin contractility.

**(Adapted from:** Basant A, Glotzer M. *Spatiotemporal Regulation of RhoA during Cytokinesis. Curr Biol.* 2018 May 7;28(9):R570-R580. doi: 10.1016/j.cub.2018.03.045. PMID: 29738735; PMCID: PMC6508076. This figure is reproduced and adapted under the Public Domain Mark 1.0 (<https://creativecommons.org/publicdomain/mark/1.0/>)

Ect2 is the primary GEF responsible for the activation of RhoA during cytokinesis.<sup>56</sup> It localizes to the cell equator and functions as a guanine nucleotide exchange factor for RhoA, catalyzing the exchange of GDP for GTP<sup>57</sup>. MgcRacGAP (also known as CYK4) plays a dual role in regulating RhoA. This challenges the traditional view that GAPs only terminate RhoA signalling, as MgcRacGAP is essential for maintaining a focused zone of RhoA activity throughout cytokinesis<sup>58</sup>. Zanin et al. have identified Rho GTPase-Activating Protein 11A (ARHGAP11A), another member of the RhoGAP family, as a critical regulator of RhoA during cell division. In contrast to the typical RhoGAPs, ARHGAP11A localizes to the plasma membrane during the early stages of mitosis and to the equatorial membrane during anaphase, indicating a specific role in cytokinesis. This study identified ARHGAP11A, designated MP-GAP(M-phase GAP), as the primary GAP targeting RhoA during mitosis and cytokinesis. Furthermore, the inhibition of MP-GAP has been demonstrated to result in the formation of large ectopic protrusions, similar to those observed in cells with constitutively active RhoA expression. Additionally, this inhibition has been shown to induce a significant level (~20%) of cytokinesis failure, predominantly due to abscission failure rather than issues with contractile ring assembly or constriction<sup>59</sup>.

MP-GAP has been demonstrated to regulate the spatial distribution of active RhoA during cell division, thereby contributing to the proper formation and ingression of the cleavage furrow.<sup>60</sup> The equilibrium between RhoA activation by GEFs and its deactivation by GAPs such as MP-GAP, as shown in Figure 5 is essential for ensuring the appropriate progression of cytokinesis. At the onset of cytokinesis, activated RhoA regulates downstream effectors, including Rho kinase, Anillin, and Formin, to promote actomyosin ring assembly and contraction, leading to cleavage furrow formation. GAPs such as MP-GAP, accelerate the hydrolysis of GTP to GDP,

deactivating RhoA and ensuring proper regulation of its activity. The process progresses through cleavage furrow maturation, midbody formation, and finally, abscission, resulting in the separation of daughter cells. An imbalance in this regulatory process can lead to cytokinesis failure and the formation of multinucleated cells or aneuploidy.<sup>56</sup>

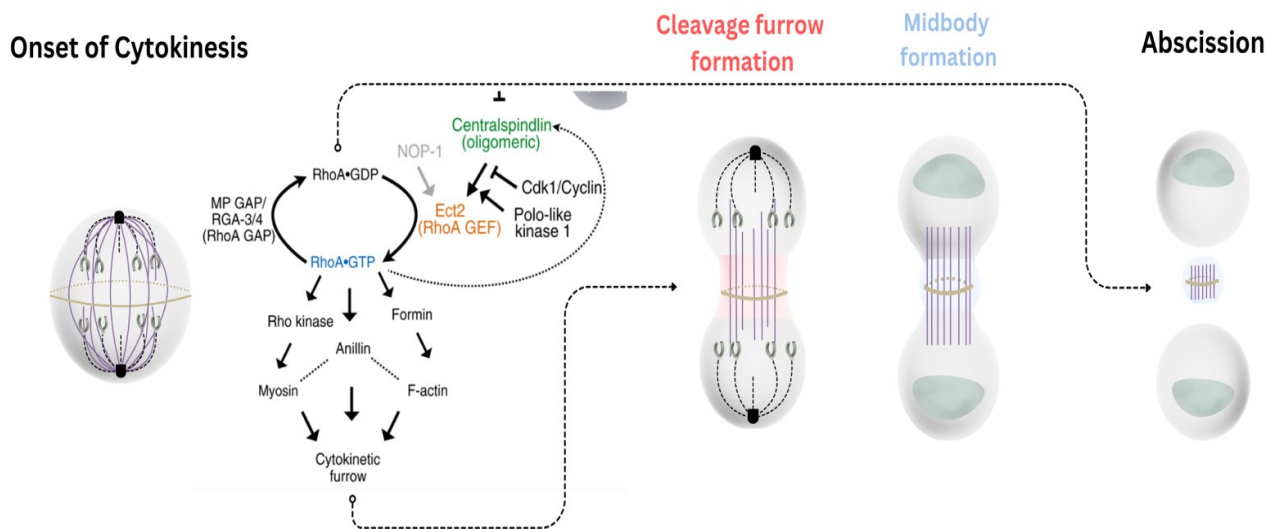


**Figure 5. RhoA Regulation and Its Role in Cytokinesis**

The figure illustrates the role of RhoA in cytokinesis, emphasizing its activation by RhoA GEFs (e.g., Ect2) and inactivation by RhoA GAPs (e.g., MP-GAP). Activated RhoA (RhoA-GTP) coordinates downstream effectors, including Rho kinase, Anillin, and Formin, to facilitate actomyosin ring assembly and contraction during cleavage furrow formation. The activation of Ect2, a RhoA GEF, is regulated by the Centralspindlin complex, which consists of key components that help recruit Ect2 to the equatorial cortex. Centralspindlin's function is modulated by Cdk1/Cyclin and Polo-like kinase 1, which regulate its oligomerization and localization, ensuring precise spatial and temporal control of cytokinesis. As the cleavage furrow ingresses, the midbody structure forms, serving as a platform for abscission machinery, ultimately leading to the final separation of daughter cells.

(Adapted from: Basant A, Glotzer M. *Spatiotemporal Regulation of RhoA during Cytokinesis*. *Curr Biol*. 2018 May 7;28(9):R570-R580. doi: 10.1016/j.cub.2018.03.045. PMID: 29738735; PMCID: PMC6508076. This figure is reproduced and adapted under the Public Domain Mark 1.0 (<https://creativecommons.org/publicdomain/mark/1.0/>)

## **1.7 Rationale and Objectives of the Predicted PKD3 and ARHGAP11A(MP-GAP) Interaction**

More recent research by the Leitges group has revealed that PKD3 is localized to the furrow during cytokinesis, where it exhibited an overlap with the F-actin ring at the equatorial plate. This suggests a potential role for PKD3 in the regulation of the contractile ring dynamics. The localisation was found to be dependent on the presence of PKC $\epsilon$ , thereby indicating a functional relationship between these two protein kinases in the regulation of cytokinesis. Genetic mutations and complementation assays demonstrated that PKD3 plays a non-redundant role in cytokinesis. Reintroduction of PKD3 into PKD3-deficient cells restored furrow localization and rescued the double/multi-nucleated phenotype, indicating failure of cytokinesis. Further insights into the activation status of PKD3 during cytokinesis were gained using phospho-specific antibodies. The results demonstrated that PKD3 exhibits distinct localization patterns during various stages of cytokinesis, indicating that its activity is subject to dynamic regulation throughout the process. It is noteworthy that the observation of activated PKD3 localizing to the midbody, a critical structure in cytokinesis, suggests its involvement in late-stage events such as abscission. Furthermore, the interaction between PKD3 and RhoA was examined. Through immunofluorescence assays and biochemical analyses, a close spatial relationship between PKD3 and RhoA was observed, particularly at the midbody. This finding suggests that PKD3 may play a role in regulating RhoA activity. It is noteworthy that the absence of PKD3 in MEFs resulted in the prolonged activation of RhoA, indicating a potential function for PKD3 in facilitating the timely deactivation of RhoA to promote abscission. One objective of the Leitges lab is to ascertain whether PKD3 exerts an indirect regulatory influence over RhoA by interacting with one of its regulators. Given that GAPs are responsible for the inactivation of

**RhoA, we hypothesise that PKD3 interacts with ARHGAP11A (MP-GAP), the primary GAP involved in regulating RhoA during abscission, as demonstrated in the Zanin et al. publication.** <sup>59</sup>

By elucidating this interaction, we aim to gain deeper insights into the molecular mechanisms of cytokinesis and their broader implications in tumorigenesis. This thesis focuses on studying the potential interaction between PKD3 and MP-GAP, utilizing the co-immunoprecipitation approach. Co-IP is a widely recognized and frequently used technique for investigating protein-protein interactions. While it has certain limitations, such as difficulty detecting weak or transient interactions and susceptibility to nonspecific binding, it remains the gold standard due to its ability to directly identify interactions under near-physiological conditions. The method provides a starting point for validating hypothesized interactions and lays the foundation for exploring protein complexes further with complementary techniques.

To establish the tools needed for the expression of both proteins in mammalian cell lines for downstream assays such as co-immunoprecipitation, we have developed a system involving epitope tags to facilitate their detection and analysis.

## Chapter II- Materials and Methods

### 2.1 Cell Lines and Cell Culture

COS-7 (African Green Monkey), CHO-K1 (Hamster), and HEK293 (Human), were utilized in this study for various experimental purposes. Stable cell HEK293 cell lines expressing PKD3-FLAG and MP-GAP-FLAG were generated in-house by our research assistant, Uschi Braun, using viral transfection methods as presented below.

COS-7 cells (ATCC, CRL-1651) were maintained in Dulbecco's Modified Eagle's Medium (DMEM)-high glucose (MilliporeSigma, Cat# D5796-500ML) supplemented with 10% fetal calf serum (FisherScientific, Cytiva, Cat# SH3412IH345), 1% penicillin-streptomycin (Pen Strep) (FisherScientific, Gibco, 15070-063),  $\beta$ -mercaptoethanol (FisherScientific, Gibco, Cat# 21985023). These cells were cultured at 37°C with 5% CO<sub>2</sub> and were passaged in 10 cm plastic dishes or 6-well dishes at a 75-85% confluence.

CHO-K1 cells (ATCC, CCL-61) and HEK293A cells (ATCC, CRL-1573) were cultured in the same medium mentioned and grown under the same incubator conditions and were subcultured upon reaching 75-90% confluency.

#### 2.1.1 Stable Cell Lines

HEK293 cell lines stably expressing PKD3-FLAG and MP-GAP-FLAG were created by viral transfection. Viral transfection was performed with the Lenti-vpak Packaging Kit (OriGene, Cat# TR30037) and Lenti-X™ 293T Cell Line (Takara, Cat #632180). Transfection was performed

according to the manufacturer's protocol. After transfection, the culture medium was replaced, and viral supernatants were collected at 48- and 72-hours post-transfection. The supernatants were filtered through a 0.45 µm PES filter (MilliporeSigma, Cat#SLHP033NS) to remove cellular debris.

Target HEK293 cells were then transduced with the filtered viral supernatants in the presence of polybrene from the Lenti-vpak Packaging Kit (OriGene, Cat# TR30037) (final concentration of 8 µg/mL) to enhance transduction efficiency. Following transduction, cells were selected using the appropriate antibiotic (e.g., puromycin (ThermoFisher, Gibco, Cat# A1113802) or G418 sulfate (ThermoFisher, Gibco, Cat# 10131027)) to establish stable cell lines expressing the desired FLAG-tagged proteins. The selection process continued for 1 to 2 weeks to ensure stable integration and expression of the transgenes.

All procedures were conducted under Biosafety Level 2 (BSL-2) conditions, adhering to institutional guidelines for handling lentiviral vectors. The resulting stable cell lines were maintained in the 10% FCS complete medium supplemented with puromycin (ThermoFisher Scientific, Gibco, Cat # A1113802) and cultured in a humidified incubator at 37°C with 5% CO<sub>2</sub>.

## **2.2 Plasmids and Constructs**

The pcDNA3.1-PKD3-C-terminal-FLAG (Clone ID: OHu35345, Accession Number: XM\_024452777.1) and pcDNA3.1-MP-GAP-C-terminal-FLAG (Clone ID: OHu10733 , Accession Number: NM\_014783.6 ) plasmids were sourced from GenScript and were used as initial templates to amplify the cDNA of PKD3 and MP-GAP, respectively using primers mentioned in Table 1. These amplified cDNAs were subsequently cloned into pcDNA3.1-C-

terminal-GST plasmid, which was obtained from Addgene (Plasmid # #128025) to create GST-tagged versions for protein expression and purification experiments.

In addition to the FLAG-tagged constructs, the pcDNA3.1-TRIM47-C-terminal-MYC plasmid, sourced from GenScript (Clone ID: OHu05456, Accession Number: NM\_033452.3) was used to express TRIM47 with a C-terminal MYC tag, allowing for MYC-specific detection. Another construct, pcDNA3.1-MP-GAP-C-terminal-HA, was sourced from GenScript (Clone ID: OHu10733, Accession Number: NM\_01478.3) and used to express MP-GAP with a C-terminal HA tag using the same pcDNA3.1 backbone, facilitating HA-specific detection in co-expression and interaction assays. All constructs were verified by Sanger sequencing and restriction digest analysis, to confirm the accuracy of the cloned sequences. These plasmids were stored at -20°C in TE buffer. For transfections, plasmid DNA was prepared using the Plasmid Midi Kit (Qiagen, Cat #12143) following the manufacturer's protocol to ensure high purity suitable for cellular transfections.

## **2.3 Cloning**

### **2.3.1 Amplification of PKD3 and MP-GAP Sequences**

PCR amplification was employed using Biometra TRIO Combi (Analytik Jena, Cat# 846-2-070-724) thermal cycler and the parameters mentioned in Table 2 to amplify the mouse PKD3 and human MP-GAP cDNAs from the original constructs obtained from GeneScript's pcDNA 3.1 mammalian expression vector containing FLAG epitope tag which was mentioned earlier. Primers specific to the target genes were designed, and PCR was performed under optimized

conditions using a Platinum <sup>TM</sup>SuperFi<sup>TM</sup> II PCR kit (Invitrogen, Cat# 12361250). An additional round of PCR was conducted using JumpStart<sup>TM</sup> Taq ReadyMix<sup>TM</sup> (Sigma Aldrich, Cat# P2893).

Gel electrophoresis analysis in 1% agarose gels with GelRed® nucleic acid stain (Biotium, Cat# 41003) in 1X TAE buffer (40 mM Tris, 1 mM EDTA, and 20 mM Acetic Acid) ran for 35 min at 110 V was used to confirm the successful amplification of the target fragments.

**Table 1. Primers Used for Fragment Amplification in GST and Lentiviral Construct Cloning**

Fragment	Forward Sequence (5' to 3')	Reverse Sequence (5' to 3')
mPKD3	gaagcttGCCACCATGTCTGCAAATAATTCC	cggatccAGGATGCTCCTCCATGTCGTC
hMP-GAP	GCTCGGATCCGCCACCATGTGG	ggatccCAAATCTACAGGTTTACTTG
Lenti-mPKD3	gaatccGCCACCATGTCTGCAAATAATTCC	ctcgagcggccgCAAATCTACAGGTTTAC
Lenti-hMP-GAP	GCTCGGATCCGCCACCATGTGG	ctcgagcggccgCAAATCTACAGGTTTAC

**Table 2. PCR Parameters**

PCR Step	Temperature (°C)	Time (Minutes)	Number of Cycles
Initial Denaturation	95°C	2 minutes	40
Denaturation	95°C	30 seconds	
Annealing	52°C	30 seconds	
Extension	72°C	2 minutes	
Final Extension	72°C	5 minutes	

### 2.3.2 TOPO TA Subcloning

After PCR amplification, the resulting products were ligated into TOPO vectors using the pCR®-2.1 TOPO® TA cloning vector (Invitrogen, Cat# 45-0641). This kit facilitates the efficient cloning of PCR products into the vector without the need for restriction enzymes. Following ligation, the reaction mixtures were transformed into One Shot™ TOP10 chemically competent *Escherichia coli* (Invitrogen, Cat# C404003), as per the manufacturer's guidelines. The transformed bacteria were plated onto LB agar plates supplemented with 100 µg/mL ampicillin to select for bacterial colonies carrying the recombinant TOPO plasmids. These plates were further enriched with 0.2 mg/mL of X-Gal (ThermoScientific, Cat# R0404) and 1 mM IPTG (Invitrogen, Cat # 15529019), facilitating the screening of clones with the correct insertions. Minipreps of the recombinant TOPO plasmids, identified by the blue-white screening method, were extracted from the selected colonies. The concentration and purity of the extracted plasmid DNA were assessed using a NanoDrop™ spectrophotometer (ThermoFisher, Cat# ND-2000).

### 2.3.3 Cloning into Mammalian Expression Vector containing GST Tag

The huMP-GAP and mPKD3 sequences obtained in earlier steps were cloned into a pcDNA3-C-terminal GST obtained from Addgene (#128025). Initially, the inserts were excised from the TOPO vector. In the case of MP-GAP, the insert was excised using the BamHI (NEB, Cat# R0136) restriction enzyme, while for PKD3, a double digestion using BamHI and HindIII (NEB, Cat #R0104) enzymes was performed. Subsequently, the excised inserts were separated via gel electrophoresis, and the gel bands containing only the inserts were excised and purified using

PureLink™ Quick Gel Extraction Kit (Invitrogen, Cat# K210012) following the manufacturer's instructions. The purified inserts were then ligated into the pcDNA3.1-C-terminal-GST vector, which had been linearized through BamHI or BamHI /HindIII digestion and dephosphorylated using the Antarctic phosphatase (AnP) (NEB, Cat# M0289) in AnP Buffer following a 3h incubation at 37°C and, further, inactivation at 85°C. For ligation, the reaction mix was prepared with T4 DNA ligase (NEB, Cat# M0202), 10X T4 DNA ligase buffer (NEB, Cat# B0202), 1.5 µL of linearized vector, and 2 µL mPKD3 or hMPGAP insert DNA at a 1:4 ratio of linearized vector to insert. The ligation mix was incubated overnight at 16°C. Subsequently, the recombinant plasmids were transformed into chemically competent *E. coli* DH5α (ThermoFisher, Cat# 18265017). The transformed cells were inoculated onto LB agar plates supplemented with 100 µg/mL ampicillin and incubated overnight at 37°C.

Colonies containing the correct plasmids were selected and validated through both sequencing analysis and restriction enzyme digestion. Restriction enzyme digestion verified the insert and its orientation, ensuring the cloned constructs' integrity for downstream applications. For sequencing analysis, 1.5 µg recombinant GST plasmid of each construct was sent to The Center of Applied Genomics (<http://www.tcag.ca>). Primer solutions corresponding to the suggested primers for sequencing were prepared per TCAG's instructions.

**Table 3. Restriction Enzymes used in Plasmid linearization and validation for GST vector constructs**

<b>Construct</b>	<b>Linearization</b>	<b>Insertion Validation</b>	<b>Orientation Validation</b>
TOPO_PKD3	-	BamHI/HindIII	-
TOPO_MP-GAP	-	BamHI	EcoRI/HindIII
pcDNA3.1_GST	BamHI/HindIII	-	-
	Bam HI		
pcDNA3.1_PKD3_GST	-	BamHI/HindIII	-
pcDNA3.1_MP-GAP_GST	-	BamHI	EcoRI/HindIII

#### 2.3.4 Cloning into Lentiviral Production Vector for Establishing Stable Cell Lines

Similar to the initial cloning process, the amplified inserts were excised from the TOPO vector. For MP-GAP, the insert was excised using the BamHI restriction enzyme, whereas for PKD3, a double digestion with EcoRI (NEB, Cat #R0101L) and NotI (NEB, Cat# R0189S) enzymes was performed. Subsequent gel electrophoresis allowed for the isolation and purification of the gene inserts using the PureLink™ Quick Gel Extraction Kit. The purified inserts were then ligated into the lentiviral production vector, which had been linearized through EcoRI and NotI double digestion for PKD3 insertion and BamHI and NotI for MP-GAP insertion. Before ligation, the resulted vector mixture underwent dephosphorylation using Antarctic phosphatase (AnP) to

prevent self-ligation. The ligation mixture, comprising T4 DNA ligase, 10X T4 DNA ligase buffer, the linearized lentiviral vector, and the inserts at a specified ratio (1:3 or 1:5 vector-to-insert), was incubated overnight at 16°C. Following ligation, the recombinant plasmids were transformed into chemically competent *E. coli* DH5 $\alpha$  cells and plated onto LB agar plates supplemented with ampicillin. Colonies containing the correct plasmids were selected and subjected to validation through *Stu*I (NEB, Cat #R0187S) digestion. Furthermore, the integrity and accuracy of the cloned constructs were verified through sequencing analysis.

**Table 4. Restriction Enzymes used in Plasmid linearization and validation for Lentiviral vector constructs**

Construct	Linearization	Insertion Validation	Orientation Validation
TOPO_PKD3	-	EcoRI/NotI	-
TOP_MP-GAP	-	BamHI/NotI	-
Lenti-ps100092_FLAG	EcoRI/NotI	-	-
	BamHI/NotI		
Lenti-ps100092_PKD3_FLAG	-	ScaI/XcmI	-
Lenti-ps100092 MP-GAP_FLAG	-	<i>Stu</i> I/ScaI	-

**Table 5. General Restriction Enzyme Digestion Setup**

<b>Component</b>	<b>Volume*</b>
<b>Restriction Enzyme(s)</b>	0.5 $\mu\text{L}$
<b>10X Buffer</b>	5 $\mu\text{L}$
<b>DNA Sample</b>	3 $\mu\text{L}$
<b>Nuclease-free Water</b>	41.5 $\mu\text{L}$
<b>Total Reaction Volume</b>	50 $\mu\text{L}$

\*For double digestion, the volumes change to accommodate the addition of a second enzyme, and other calculations adjust accordingly.

## **2.3 Expression of epitope-tagged proteins**

### **2.3.1 Transfection**

Transient transfections were conducted in mammalian cells using Lipofectamine™ (Invitrogen, Cat # 18324020) and Lipofectamine 3000 (Invitrogen, Cat # L3000001) according to the manufacturer's instructions. Briefly, mammalian cells were seeded in appropriate culture vessels (Six-well dish, ThermoFisher, Cat #FB012927) and allowed to reach the desired confluency (70-85%) before transfection. The cloned plasmids were prepared for transfection according to standard procedures, including purification and quantification to ensure consistent transfection efficiency. Transfection complexes were formed by mixing the purified plasmids with Lipofectamine reagent in Opti-MEM™ Reduced Serum Medium (Gibco, Cat # 31985070) followed by a brief incubation period to allow for complex formation. The transfection

complexes were then added to the cells and incubated for the specified duration. 24-48 hours post-transfection, the transfected cells were harvested for analysis of fusion protein expression.

## 2.4 Western Blotting

**Table 6. Antibodies and dilutions used for immunoblotting**

<b>Primary Antibody</b>	<b>Isotype</b>	<b>Manufacturer</b>	<b>Catalog Number</b>	<b>Dilution</b>
FLAG (THE™ DYKDDDDK Tag Antibody)	Mouse	GenScript	A00187	1:1000
GST (HRP Conjugated)	Rabbit	Cell Signaling Technology	5475S	1:1000
GAPDH	Rabbit	Cell Signaling Technology	3683	1:1000
Myc (THE™ c-Myc Tag Antibody)	Mouse	GenScript	A00704S	1:750
HA (THE™ HA Tag Antibody)	Mouse	GenScript	A01244S	1:1000
<b>Secondary Antibody</b>	<b>Isotype</b>	<b>Manufacturer</b>	<b>Catalog Number</b>	<b>Dilution</b>
Anti-mouse IgG (HRP)	Mouse	Cell Signaling Technology	7076S	1:2000

#### 2.4.1 Cell lysis, Protein Extraction, Protein Quantification

Cells grown in a six-well plate were detached by adding 500  $\mu$ l of 1X trypsin [FisherScientific, Gibco, 0.5% Trypsin-EDTA (10X), Cat# 15400054] and incubating at 37°C for 5–10 minutes, depending on the adherence properties of the cell line. The detached cells were transferred to a microtube, and an equal volume of DMEM/ 10% FBS was added to neutralize the trypsin. The cells were centrifuged at 2000 rpm for 5 minutes, and the resulting pellets were washed twice with ice-cold phosphate-buffered saline (MilliporeSigma, Dulbecco's, Cat# D8537) to remove residual media. Cell lysis was performed using different lysis buffers, the compositions of which are listed in the Table 7 below. These buffers, supplemented with a protease inhibitor cocktail (Roche- EDTA free Protease Inhibitor Cocktail tablets, Cat# 04693159001), were added to the cell pellets, and the lysates were incubated on ice for 10–15 minutes to ensure efficient cell lysis. Following the incubation, the lysates were centrifuged at maximum speed for 15–20 minutes at 4°C, and the supernatants containing soluble proteins were collected. The protein concentration was determined using the Bradford assay following the manufacturer's instructions (MilliporeSigma, Bradford Reagent, Cat# B6916-500).

**Table 7. Cell Lysis Buffer Composition**

Lysis Buffer Name	Ingredients	Manufacturer
RIPA	50 mM Tris-Hcl, pH 7.5, 150 mM NaCl, 1% Triton x-100, 1% sodium deoxycholate (NaDOC), 0.1% sodium dodecyl sulfate (SDS), and 2 mM EDTA	Made in-house
Pierce™ IP Lysis Buffer	25 mM Tris-HCl pH 7.4, 150 mM NaCl, 1 mM EDTA, 1% NP-40 and 5% glycerol	Thermo Scientific (Cat#87787)

#### 2.4.2 SDS-PAGE

The collected lysates were denatured by adding SDS-PAGE loading buffer [125 mM Tris-HCl (pH 6.8), 4% (w/v) SDS, 20% (v/v) glycerol, 10% (v/v)  $\beta$ -mercaptoethanol, and 0.02% (w/v) bromophenol blue] and boiled at 96°C for 5 minutes in an Eppendorf ThermoMixer to ensure protein denaturation and uniformity in protein structure. Given the high molecular weight of both PKD3 and MP-GAP proteins, 8% acrylamide gels were hand-cast for protein separation. To maintain consistency and accuracy in protein loading, equal amounts of total protein (20  $\mu$ g per lane) were loaded into each well of the gel in a total volume of 20–30  $\mu$ L per sample. The gels were then subjected to electrophoresis at 110V for one hour and 45 minutes to ensure the efficient separation of proteins based on their molecular weight. This voltage and duration were selected to achieve optimal resolution and minimize any potential smearing or distortion of protein bands during electrophoresis. Following electrophoresis, the separated proteins were ready for subsequent transfer onto a nitrocellulose membrane for western blot analysis or Ponceau S staining for visualization.

### 2.4.3 Immunoblotting

After protein separation by SDS-PAGE, the proteins were transferred onto a nitrocellulose membrane using a wet transfer system. For wet transfer, a sandwich was prepared with the gel, membrane, and filter papers and placed in a western blot tank (Hoefer Mighty Small transfer unit). The transfer was conducted at 400 mA for 1 hour at room temperature to ensure efficient transfer of proteins from the gel to the membrane. Following the transfer, the membrane was blocked in a 5% (w/v) skimmed milk prepared in PBS with 0.01% (v/v) Tween-20 (PBS-T) buffer to prevent the non-specific binding of antibodies. The blocking step was carried out either overnight at 4°C or for two hours at room temperature to allow for thorough blocking of the membrane. After blocking, the membrane was incubated with the primary antibody specific to the epitope tags. This incubation was performed overnight at 4°C with gentle agitation to ensure complete and specific binding of the primary antibody to its target protein. Subsequently, the membrane was washed three times with PBS-T (PBS + 0.01% Tween-20) for 30 minutes in total to remove any unbound primary antibody. Following the washes, the membrane was then incubated with a secondary antibody conjugated to HRP for 2 hours at room temperature.

### 2.4.4 Western Blot Imaging

After incubation with the secondary antibody, the membrane was washed again to remove any unbound secondary antibody, and the target protein bands were visualized using the chemiluminescence method. A SuperSignal™ West Pico Plus Chemiluminescent Substrates Kit (Thermo Fisher Scientific, Cat# 34580), was applied onto the membrane, covering the protein bands. Imaging of the chemiluminescent signal was conducted using the Analytic Jena UVP Chem

Studio Plus machine. To capture the chemiluminescent signal, images were taken at different exposure times based on the signal intensity of the protein bands. Shorter exposure times were used for highly intense bands to prevent overexposure and saturation of the signal, while longer exposure times were employed for fainter bands to enhance their visibility. The molecular mass of the proteins analyzed in this study are as follows: the FLAG tag is approximately 1 kDa, the GST tag is approximately 26 kDa, PKD3 has an estimated molecular weight of 110 kDa, and MP-GAP is approximately 115 kDa. These values were considered during the interpretation of Western blot results to ensure accurate identification of the expected protein bands.

## **2.5 Immunoprecipitation**

The immunoprecipitation steps were performed following the GenScript Anti-DYKDDDDK Affinity Resin Easy (Cat. No. L00907) protocol. The reagents used for these steps were prepared according to the recipes provided in the protocol. TBS (50 mM Tris-HCl, 150 mM NaCl, pH 7.4) was used for equilibrium. TBST (TBS with 0.05% Tween-20) was used for washing steps. The resin slurry was mixed thoroughly on a rotator for 5 minutes to achieve a homogeneous suspension. The resin was then packed into a clean centrifuge tube using a wide pipette tip, centrifuged at 1000 g for 1 minute, and the supernatant was discarded while leaving the resin undisturbed. The settled resin volume was recorded as the bed volume. Equilibration was performed by adding 10 bed volumes of TBS buffer, centrifuging at 1000 g for 1 minute, and discarding the supernatant. This step was repeated once more.

Prepared cell lysates were added to the equilibrated resin and incubated on a rotator for 1–4 hours at room temperature. For Co-IP experiments, incubation was performed overnight at 4°C.

After centrifugation, the supernatant was collected. The resin was washed three times with TBST buffer, with each wash involving mixing and centrifugation steps (at 1000 g for 1 minute). Elution was carried out by adding an equal bed volume of SDS-PAGE sample buffer to the resin, followed by mixing and heating at 90–100°C for 5–10 minutes. After centrifugation, the supernatant was collected for subsequent analysis by SDS-PAGE and Western blotting.

## Chapter III-Results

### 3. Results

#### 3.1 Plasmid Cloning and Validations

This section presents the results and cloning strategies used to develop GST-fusion and lentiviral constructs. The GST-fusion and lentiviral constructs were established in-house, using FLAG-tagged constructs purchased at GeneScript (see 2.2 Plasmids and Constructs) as starting material. Primers for subsequent PCR-based subcloning were designed using sequences from the FLAG constructs. The FLAG, HA, and Myc-tagged constructs used in this study were purchased from GeneScript. Detailed descriptions of the cloning procedures, validation methods, and their integration into the study are provided below. In general, the strategies for obtaining the GST fusion and lentiviral constructs for this study involved multiple cloning steps.

In summary, the PCR fragments were subcloned into the pCR<sup>TM</sup>2.1-TOPO vector (From ThermoFisher TOPO TA subcloning kit) for sequence analysis and efficient subcloning later on. Appropriate inserts were then excised with specific restriction enzymes and ligated into the final expression vectors. The final constructs were validated by specific restriction enzyme digestions to confirm both the presence and correct orientation of each insert. To further ensure successful cloning, the final constructs were verified by DNA sequencing, which confirmed the correct cDNA sequences and, in particular, the correct insertion into the promoter region to ensure subsequent expression of the construct.

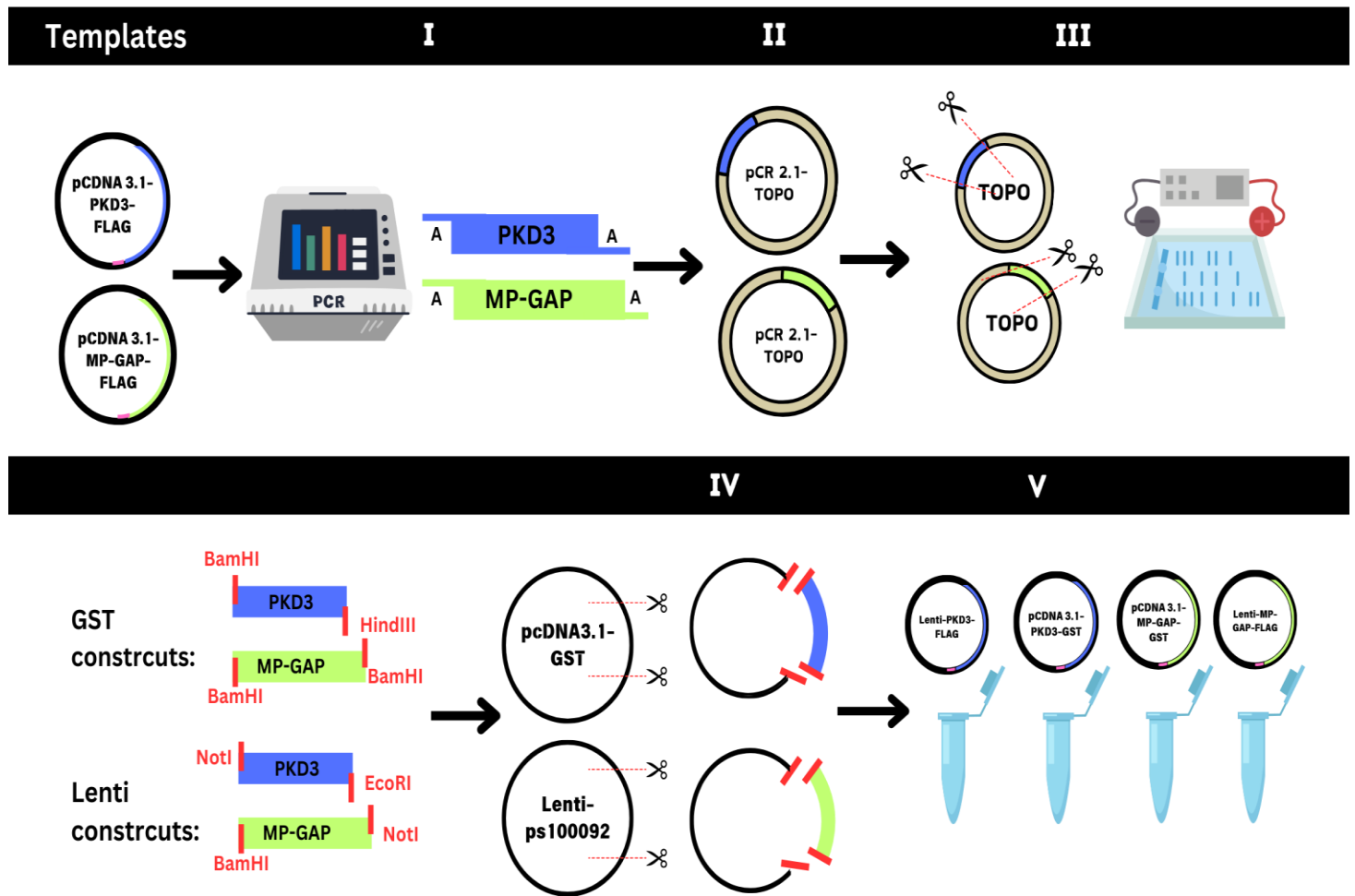


**Figure 6. Cloning Strategy for Developing GST-Tagged and Lentiviral Constructs**

The figure illustrates the cloning strategy used for the development of the GST-tagged and lentiviral constructs, broken down into five key steps. I) The protein-coding sequences for PKD3 and MP-GAP were amplified through PCR, using FLAG-tagged constructs (pcDNA3.1-PKD3-FLAG and pcDNA3.1-MP-GAP-FLAG) as templates. II) Individual PCR amplicons are subcloned into pCR 2.1-TOPO TA vector. III) Once the plasmids were isolated, gel electrophoresis was used to verify the presence of the correct constructs. IV) The inserts were then excised from the TOPO vector using the restriction enzymes mentioned. V) The purified inserts were then ligated into two final vectors: pcDNA3.1-GST and Lenti-ps100092.

### 3.1.1 GST-fusion Constructs (pcDNA3.1-mPKD3-GST, pcDNA3.1-hMP-GAP-GST)

For both constructs, the pcDNA3.1-C-terminal GST vector was used for subcloning. To enable the expression of PKD3, PCR primers were designed (see Table 1 , Chapter II) to amplify the full-length coding sequence of the mouse PKD3 gene from the template vector. The primers incorporated a HindIII restriction site at the 5' end, just upstream of the start codon (ATG), and a BamHI site at the 3' end of the coding sequence. These restriction sites were included to ensure the correct in-frame insertion of the *PKD3* cDNA downstream of the promoter region and upstream of the 3' GST-tag for subsequent protein fusion. Following successful TOPO subcloning, a restriction enzyme digest analysis was performed to verify the integrity of the insert (see Figure 7, panel A), and selected clones were subjected to Sanger sequencing to confirm the absence of mutations in the *PKD3* sequence.

The next step was to subclone the *PKD3* cDNA (the BamHI/HindIII insert) into the pcDNA3.1 C-terminal GST vector, which allows the expression of a GST-tagged PKD3 fusion protein. The presence of the correct insert in the final clones was validated by a combination of specific restriction enzyme digestion, as shown in Figure 8, panel A, and sequencing analysis to ensure correct insertion and reading frame alignment for fusion protein expression. The digestions included double digestion with BamHI and HindIII, which produced fragment sizes of 6.1 kb and 2.7 kb, consistent with the expected sizes for both the vector and the PKD3 insert, confirming successful ligation. A second digestion with PstI and PvuI further validated the insertion and orientation of the PKD3 sequence, yielding fragments of 4 kb, 2.6 kb, and 2.1 kb, which aligned with the predicted pattern.

A similar cloning strategy was followed for the *MP-GAP* to ensure a proper expression of a GST fusion protein. PCR primers were designed (see Table 1, Chapter II) to amplify the full-length coding sequence of MP-GAP from the corresponding template vector. This time BamHI restriction sites were incorporated at both the 5' and 3' ends of the coding sequence to ensure correct in-frame cloning into the vector. As with the PKD3 cloning process, the MP-GAP PCR amplified fragments were first subcloned into the pCR<sup>TM</sup>2.1-TOPO vector. The clones were verified by restriction enzyme digestion as shown in Figure 7, panel B, and sequencing analysis. Once the integrity of the sequence was confirmed, the MP-GAP cDNA insert, excised from the TOPO vector as a BamHI insert, was subcloned into the pcDNA3.1-C-terminal GST vector. The presence and correct orientation of the *MP-GAP* sequence was validated by specific restriction enzyme digestion followed by sequencing. The digestion included a BamHI digestion which yielded fragments of 6.1 kb and 3.1 kb, confirming the presence of the MP-GAP insert, and a second digestion with PstI and PvuI which validated the correct insertion and orientation, yielding fragments of 3.9 kb, 2.6 kb, 1.6 kb, 580 bp, and 510 bp, corresponding to the expected sizes as shown in Figure 8, B.

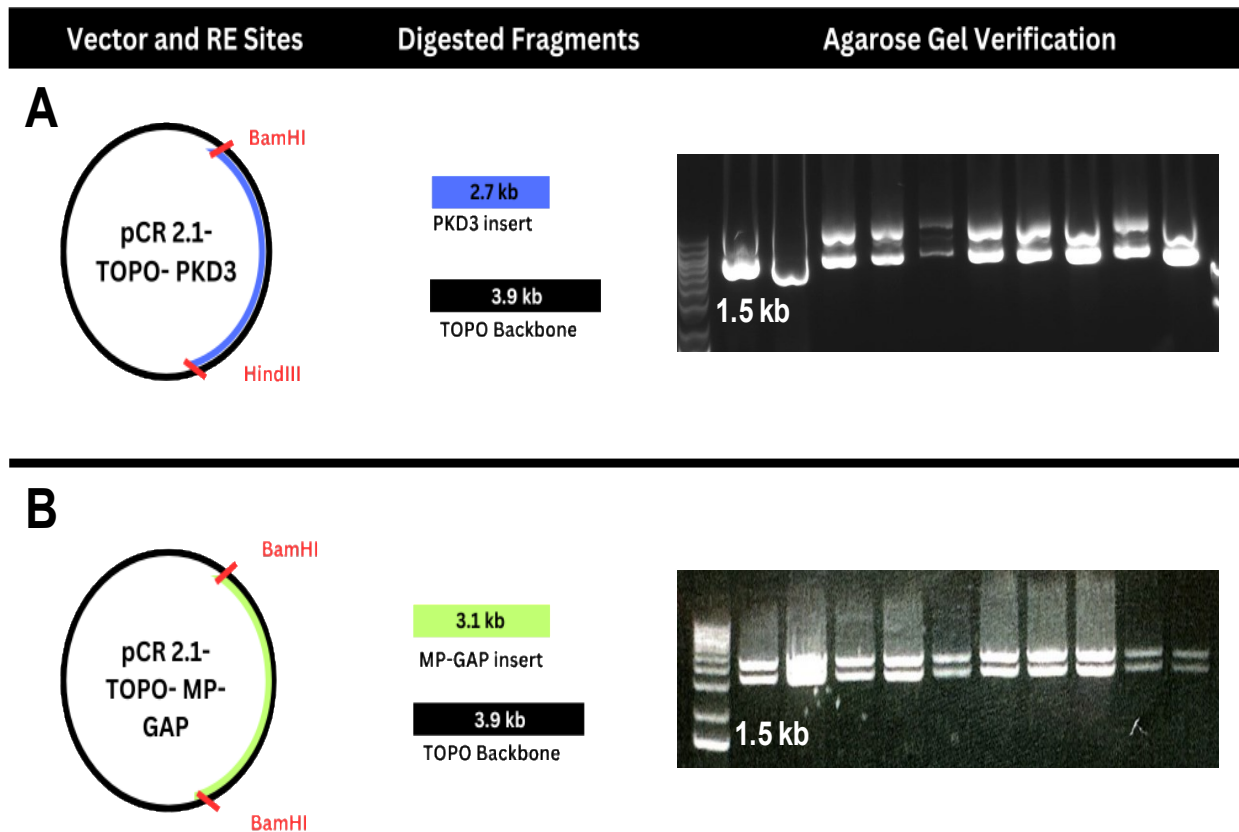


**Figure 7. Restriction Enzyme Validation of TOPO TA Subcloning Step in Cloning of GST Constructs**

The figure demonstrates the validation of the TOPO TA subcloning in cloning of GST constructs through restriction enzyme digestion and agarose gel electrophoresis. The plasmid maps for pCR 2.1-TOPO-PKD3 and pCR 2.1-TOPO-MP-GAP are shown on the left, indicating the locations of the restriction enzyme sites used for each digestion. The middle panel shows the expected fragment sizes. The agarose gel verification on the right shows the plasmid digestion pattern of selected colonies. The plasmids with matching patterns were chosen for the next step of cloning.

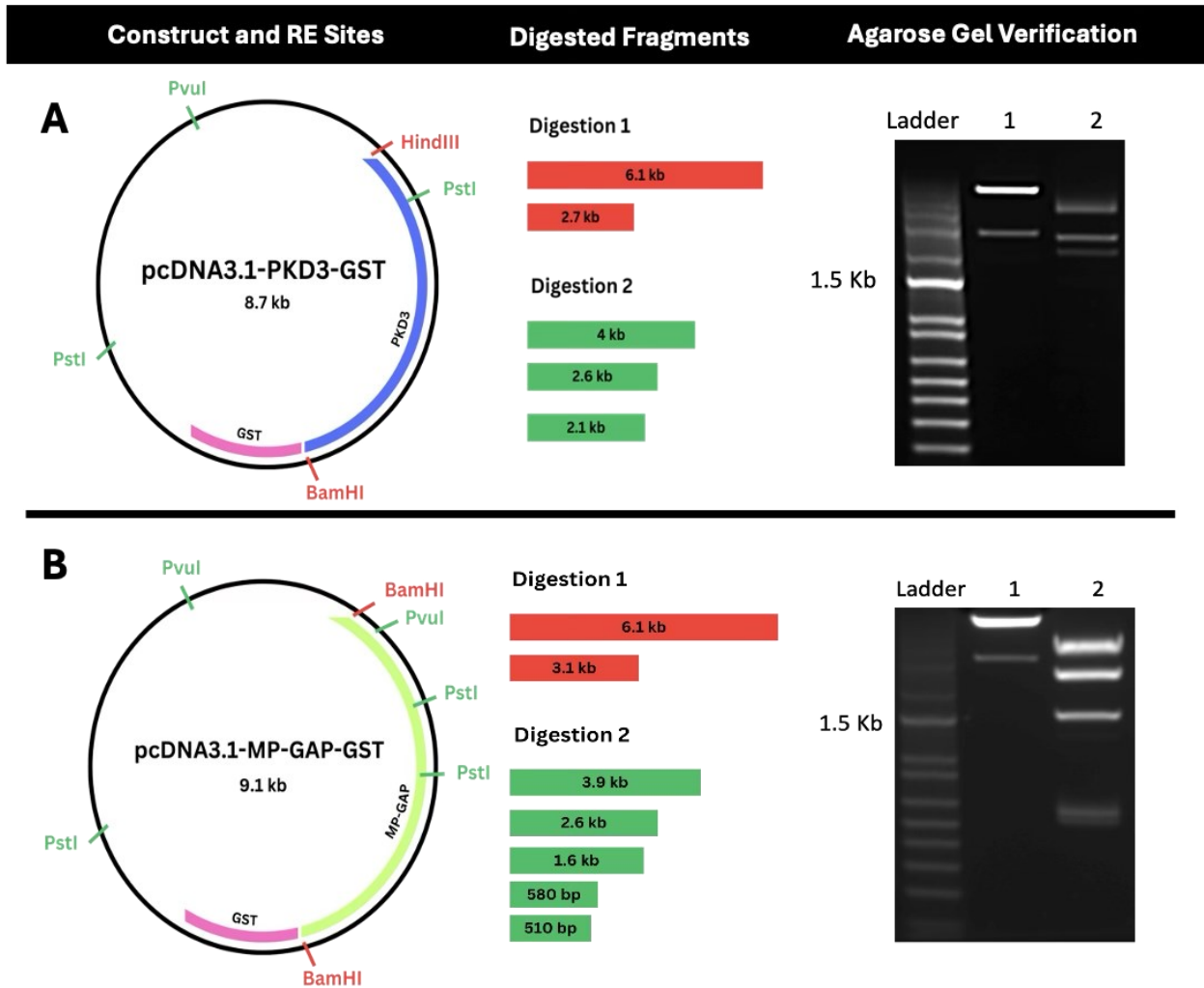


**Figure 8. GST Constructs Restriction Enzyme Validation**

This figure illustrates the validation of the final vectors obtained in GST construct cloning using restriction enzyme digestion. The plasmid maps for both GST constructs are displayed on the left, highlighting the restriction enzyme sites utilized for digestion. The middle section outlines the anticipated fragment sizes, while the agarose gel on the right validates successful digestion.

### 3.1.2 Lentiviral Constructs (psLenti-PKD3-FLAG, pLenti-MP-GAP-FLAG)

The cloning strategy for the lentiviral construct followed a similar approach to the GST fusion constructs described above, with key differences in the final expression vector. Specifically, for the lentiviral expression system, the PKD3 and MP-GAP cDNAs were subcloned into the p-Lenti\_ps100092 vector. This vector, with a total size of 7009 bp, contains a C-terminal FLAG tag and includes key functional elements such as the CMV promoter for robust gene expression, a PuroR (puromycin resistance) marker for selection in mammalian cells, and the WPRE (woodchuck hepatitis virus post-transcriptional regulatory element) to enhance transgene expression efficiency and stability. It also contains the HIV-1  $\Psi$  sequence, which is critical for efficient lentiviral packaging, enabling the production of lentiviral particles for use in the establishment of stable cell lines. These stable cell lines played a critical role in the co-IP experiments, allowing consistent expression of the proteins of interest.

As with the GST constructs, PCR primers were designed to amplify the full-length coding sequences of both PKD3 and MP-GAP from the same templates, incorporating the appropriate restriction enzyme sites (EcoRI/NotI for PKD3 and BamHI/NotI for MP-GAP) at the 5' and 3' ends to ensure accurate in-frame insertion. The individual PCR products were subcloned into the pCR<sup>TM</sup>2.1-TOPO vector and verified by restriction enzyme digestion (see Figure 9) and sequencing. After validation, the individual PKD3 and MP-GAP inserts were subcloned into the p-Lenti\_ps100092 vector, as previously indicated, and finally verified by restriction digest analysis and sequencing. For the Lenti-PKD3-FLAG construct, initial digestion with NotI and EcoRI yielded fragments of ~2.7 kb (PKD3 insert) and 7 kb (vector backbone), confirming successful insertion. Further validation using StuI gave fragments of 7.4 kb and 2.3 kb, while double digestion with ScaI and XcmI gave fragments of 4.9 kb, 3.2 kb, and 1.5 kb, confirming

correct orientation and integration of the PKD3 FLAG sequence. For the Lenti-MP-GAP-FLAG construct, digestion with BamHI and NotI yielded fragments of ~3 kb and 7 kb, confirming the MP-GAP insert. Further validation with StuI gave fragments of 8.9 kb and 1.2 kb, followed by double digestion with ScaI and StuI gave fragments of 6.4 kb, 2.5 kb, and 1.2 kb, confirming the correct insertion and orientation of the MP-GAP FLAG sequence (see Figure 10).

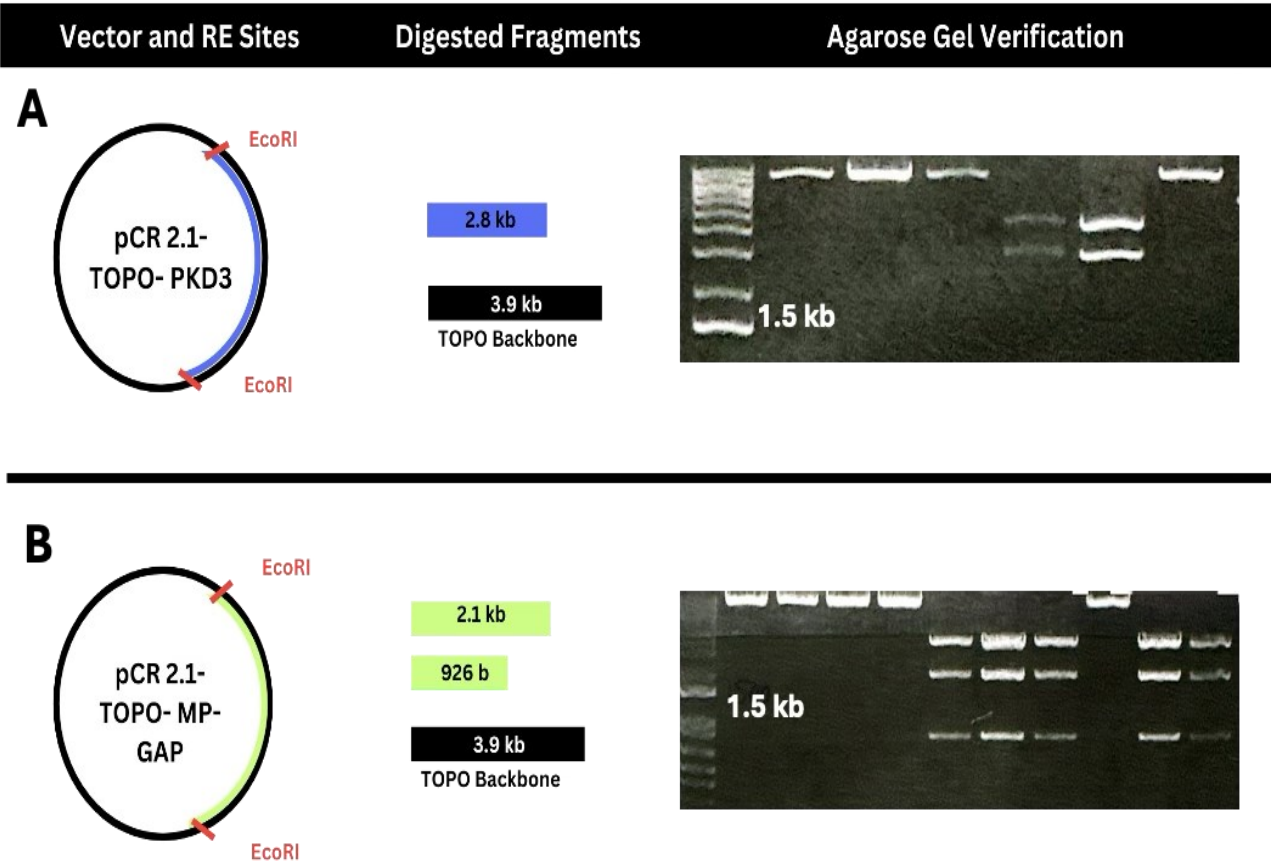


**Figure 9. Restriction Enzyme Validation of TOPO TA Subcloning Step in Cloning of Lentiviral Constructs**

The figure illustrates the validation process for TOPO TA subcloning of lentiviral constructs via restriction enzyme digestion and subsequent analysis through agarose gel electrophoresis. On the left, plasmid maps for pCR 2.1-TOPO-PKD3 and pCR 2.1-TOPO-MP-GAP highlight the specific restriction enzyme sites utilized for digestion. The central panel outlines the expected fragment sizes post-digestion, while the agarose gel results on the right show the digestion pattern of some plasmids obtained from different bacterial colonies. The plasmids with matching patterns were chosen for subsequent cloning steps.

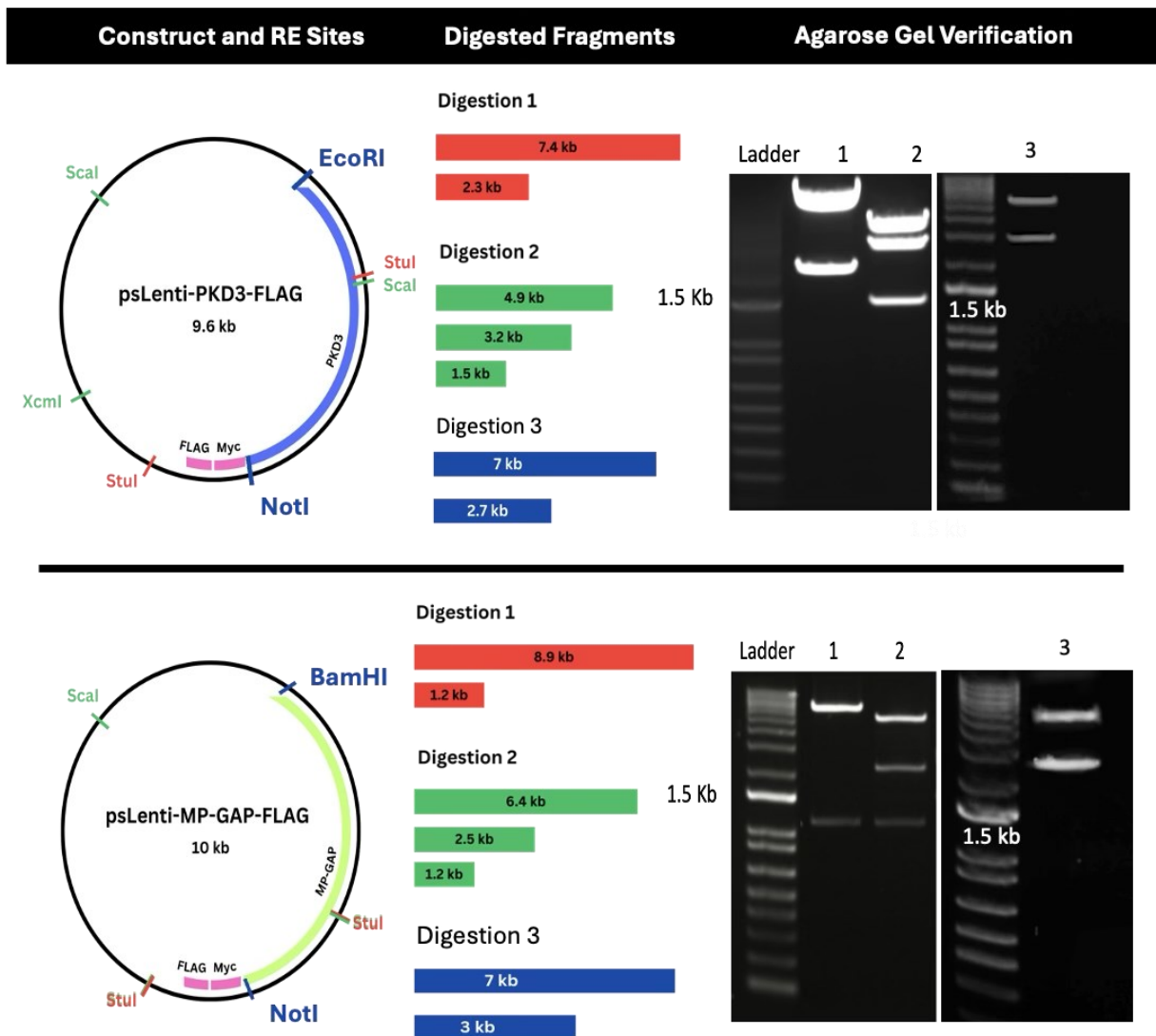


**Figure 10. Lentiviral Constructs Restriction Enzyme Digestion**

This figure shows the validation of the Lenti-PKD3-FLAG and Lenti-MP-GAP-FLAG constructs through restriction enzyme digestion. The plasmid maps for both lentiviral constructs are shown on the left, showing the restriction enzyme sites used for digestion. The middle section presents the predicted fragment sizes, while the agarose gel on the right confirms the successful digestion by clearly displaying the expected fragment separation.

### 3.2 Epitope-tagged protein transient expression

To evaluate the expression of each epitope-tagged PKD3 and MP-GAP construct, three different mammalian cell lines were tested: COS-7, CHO-K1, and HEK293. Initial transfection attempts with the pcDNA3.1-PKD3-DYK construct (GeneScript, Clone ID: OHu35345, Accession Number: XM\_024452777.1) using the Lipofectamine™ transfection reagent (Cat# 18324012) following the standard protocol provided by the manufacturer gave suboptimal results (see Figure 11). When using COS-7 and CHO-K1 cells, the results showed low exogenous protein expression as evidenced by faint bands in the subsequent Western blot. One possible reason for this was the significant cytotoxicity observed in both cell lines after transfection. Using light microscopy, a significant proportion (~50%) of the transfected cells appeared rounded up and detached from the dish after 48h, which we identified as potential apoptotic cells without further analysis. In contrast, the non-transfected control cells appeared to be healthy and showed an adherent morphology. To address this issue, we switched to Lipofectamine 3000 (Invitrogen, Cat# L3000001), a reagent designed for higher efficiency and reduced toxicity. In addition, we investigated other potential causes of the observed cell death, including visible contamination in the culture medium. Mycoplasma testing was also performed on the CHO-K1 and Cos-7 cell lines. Results confirmed mycoplasma contamination in the Cos-7 cells as shown in panel B, Figure 11. As a result, subsequent optimization efforts in this project using the new reagent were carried out using CHO-K1 and HEK293 cells only.

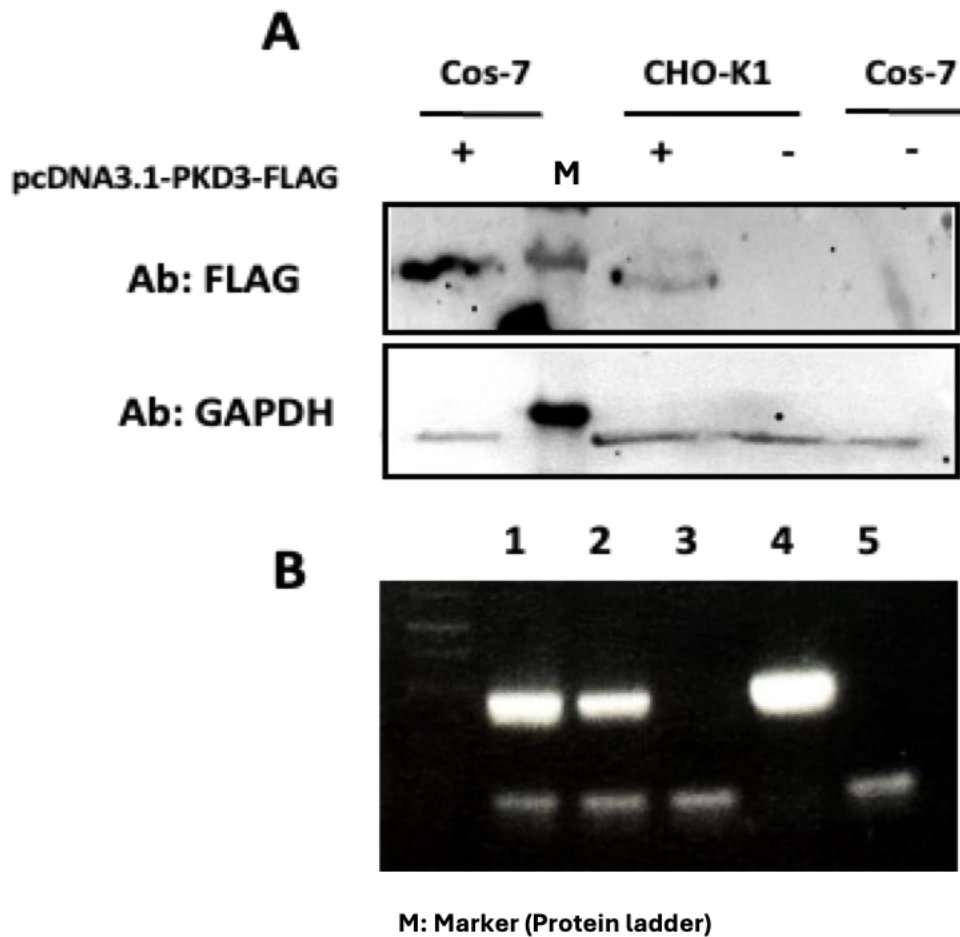
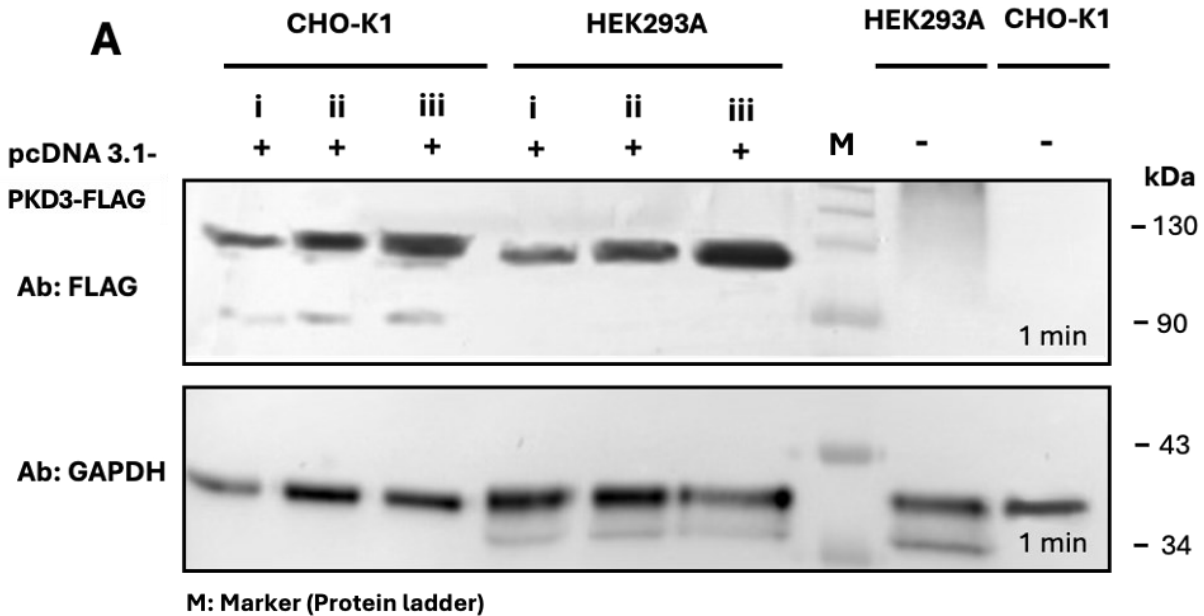


**Figure 11. Suboptimal Efficiency of Initial Transfection Experiments**

A) Western blot analysis of lysates from cells transfected with pcDNA3.1-PKD3-DYK collected from a single well of a six-well plate. The Western blot shows faint, barely detectable bands for PKD3-FLAG, indicating low protein yield following transfection. B) PCR mycoplasma test of COS-7 and CHO-K1 supernatants. 1 and 2 represent COS-7, 3 represents CHO-K1, 4 is the positive control while 5 corresponds to the negative control.

After obtaining the new transfection reagent, single transfections were performed with HEK293A and CHO-K1 cells. Microscopic examination 48 hours post-transfection showed that cytotoxicity was greatly reduced, with over 80% of both cell lines showing a healthy morphology. Having established that Lipofectamine 3000 was less toxic, a series of optimization experiments were carried out in HEK293 and CHO-K1 cells to optimize exogenous protein expression. Different concentrations of DNA and Lipofectamine 3000 were tested. As a result, as shown in Figure 12, we found that 2.5-4  $\mu\text{g}$  of plasmid DNA combined with 3  $\mu\text{l}$  of reagent per well of 6 well plate dishes gave the best results in HEK293 and CHO-K1 cells, as indicated by good to strong signals of the appropriate size in the subsequent Western blot analysis. In addition, when working with CHO-K1 and HEK293 cells, it was observed that HEK293 cells reached the desired confluence for transfection more quickly after seeding. This accelerated the transfection process and allowed for faster downstream analysis. As a result, HEK293 cells became the primary cell line for subsequent experiments due to their rapid growth and confirmed high transfection efficiency as tested in the final optimizations. Nevertheless, CHO-K1 cells were still used in selected experiments, as indicated in the relevant sections where applicable.



**B**

#Sample	Amount of DNA ( $\mu\text{g}$ )	Amount of Lipofectamine 3000 ( $\mu\text{l}$ )
i	2.5	3
ii	2.5	4
iii	4.0	3

**Figure 12. Transfection Optimization in CHO-K1 and HEK293A Cell Lines**

These experiments included titrating the DNA input from 2.5  $\mu\text{g}$  to 4  $\mu\text{g}$  and adjusting the reagent volume to identify the optimal transfection conditions that balanced high protein expression levels with minimal cytotoxicity. Through this process, we determined that using 2.5-4  $\mu\text{g}$  of DNA and 3  $\mu\text{L}$  of Lipofectamine 3000 per well in a 6-well plate provided the best transfection efficiency with negligible cell death.

### 3.2.1 Expression Discrepancy Between PKD3-FLAG and MP-GAP-FLAG in Transient Transfections

The expression level of PKD3-FLAG was consistently higher than that of MP-GAP-FLAG when transiently transfected into HEK293 cells, as shown by stronger signals in the Western blot analysis in Figure 13. This difference was consistently observed under controlled experimental conditions, including equal numbers of transfected cells, identical amounts of protein loaded on the gel, and the use of the same exposure times and imaging settings. The difference in expression levels was so significant that when both proteins were blotted on the same membrane for Western blot analysis, the strong signal from PKD3-FLAG often masked the weaker signal from MP-GAP-FLAG, or in other words, it led to over-exposure of PKD3-FLAG and under-exposure of MP-GAP-FLAG, resulting in either no detectable band or a very faint band for MP-GAP-FLAG. To overcome this, we adapted the membrane development approach in Western blotting by cutting the membrane at the regions corresponding to where each sample was loaded and imaging each section independently. This allowed optimal visualization of both PKD3-FLAG and MP-GAP-FLAG, improving the comparative analysis. Even after performing these steps and developing the membrane sections independently, the difference in expression levels remained evident. When the PKD3-FLAG membrane was developed, a strong and intense band appeared within seconds of exposure. In contrast, for MP-GAP-FLAG, under the same imaging settings, a comparable strong signal appeared only after a much longer exposure time of 2 to 5 minutes as it is shown in Figure 13.

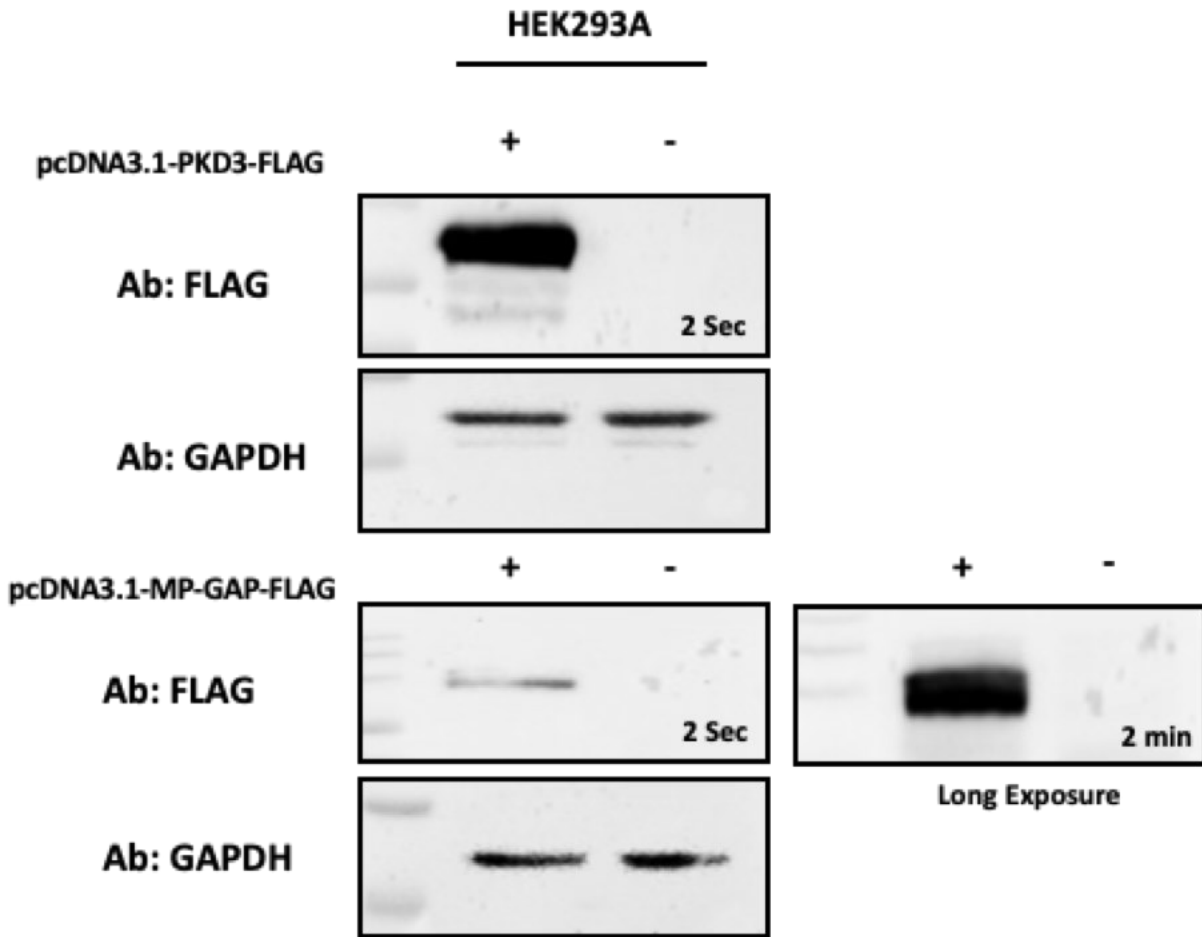


**Figure 13. Western Blot Analysis of FLAG-tagged Protein Expression in HEK293A Cells Using the Optimized Transfection Protocol**

The analysis was performed using lysates from cells transiently transfected with constructs encoding PKD3-FLAG and MP-GAP-FLAG, followed by immunoblotting with specific antibodies against FLAG. GAPDH was used as a loading control to ensure equal protein loading across the samples. The top image shows a Western blot membrane with a strong, distinct band corresponding to the PKD3-FLAG protein at approximately 100 kDa, clearly visible after 2 seconds of exposure. The bottom images illustrate the expression of MP-GAP-FLAG. A faint band is visible after a 2-second exposure. However, a prominent band appears after a 2-minute exposure.

Following the successful expression of the FLAG constructs and the optimization of the transfection protocol, the next phase of the project focused on optimization of the other constructs required for the co-immunoprecipitation experiments with the initial attempts involving GST-tagged constructs. The use of both FLAG- and a second tagged construct allows for the specific identification of interacting partners in Co-IP assays, as the tags facilitate selective binding to their respective antibodies. This dual-tagging strategy is crucial for confirming interactions between the proteins of interest and ensuring experimental specificity.

Transfection of the PKD3-GST construct transfection in HEK293A cells resulted in a detectable band on the Western blot, indicating successful protein expression. However, the MP-GAP-GST construct consistently failed to produce a reasonable or any signal on the Western blot, even after optimization efforts (see

Figure 14). Multiple attempts to enhance MP-GAP-GST expression in HEK293A cells, including variations in transfection conditions and imaging, did not yield satisfactory results. In addition, CHO-K1 cells were also transiently transfected to express MP-GAP-GST, but this also failed to produce detectable protein bands on the Western blot. Thus, the MP-GAP-GST construct was not successfully expressed in either cell line under the conditions tested. Given the lack of a reasonable expression for the MP-GAP-GST construct, we decided to proceed with a new MP-GAP construct with a different epitope tag, in case the problem was related to the presence of the GST tag. To this end, we purchased a MP-GAP-HA construct from GeneScript for subsequent experiments. The new MP-GAP-HA construct had the same expression vector backbone, pcDNA3.1, as the previous construct, but with an HA tag replacing the GST tag. This construct was then tested for expression using the optimized transfection protocol in HEK293A cells as shown in Figure14, panel C.



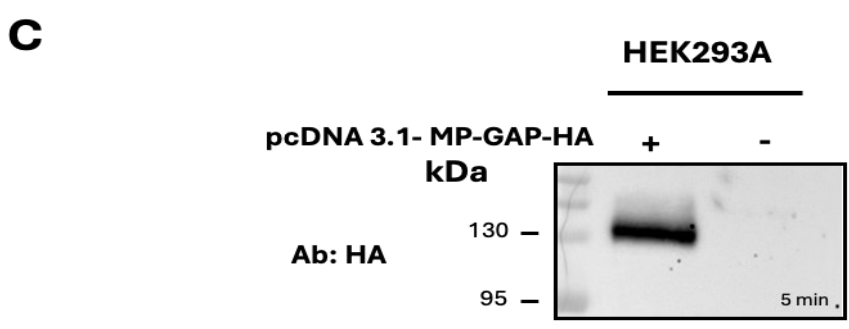
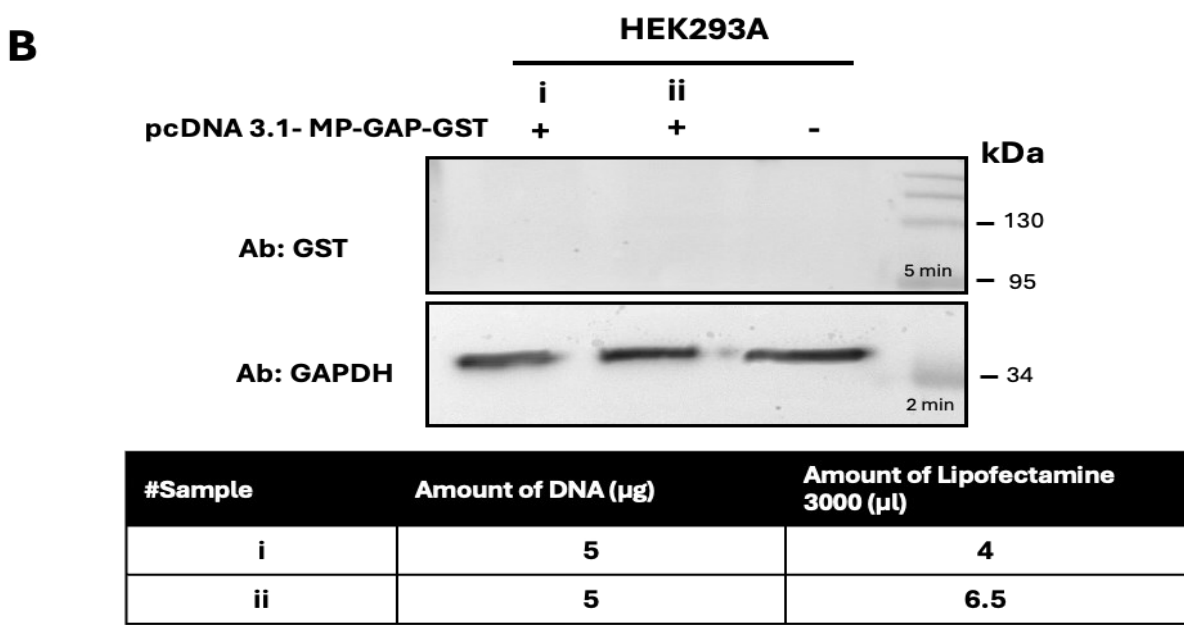
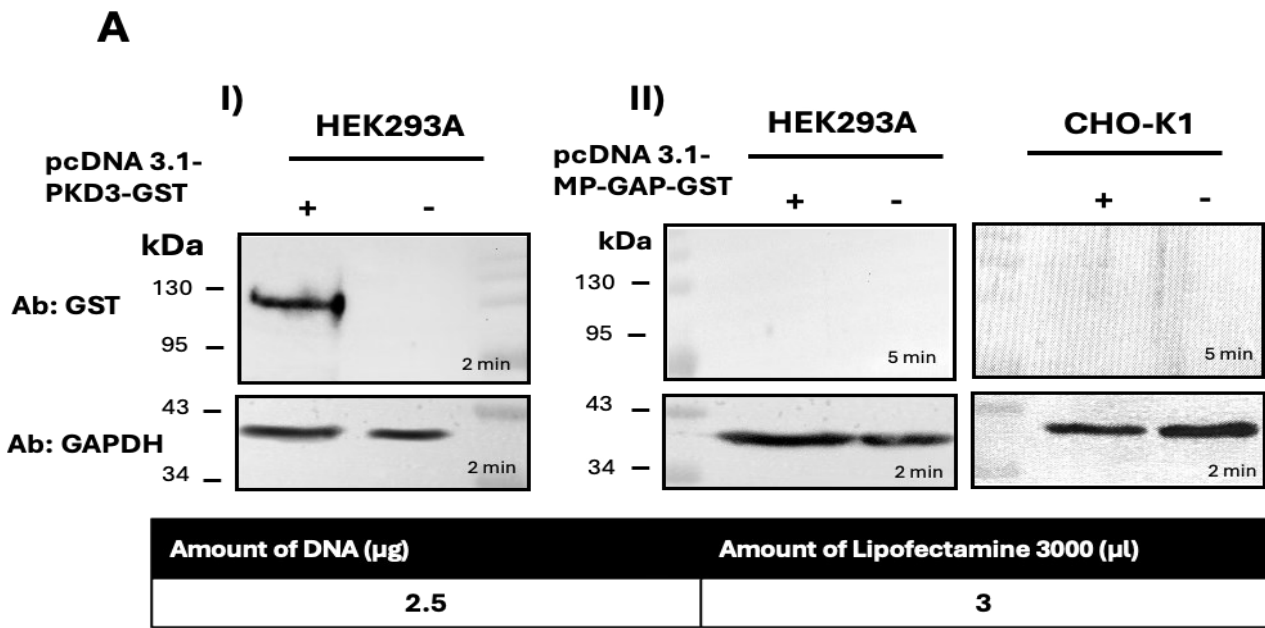


## **Figure 14. Transient Expression of GST Constructs Developed In-house and Purchased HA Construct**

Panel A, shows the expression levels of PKD3-GST and MP-GAP-GST in the indicated cell lines, following transient transfection using the amounts specified in the table below the figure. In panel B, the optimization of MP-GAP-GST expression is demonstrated, using various amounts of DNA and transfection reagent, as indicated in the table beneath the figure. Finally, in panel C, the expression of the purchased MP-GAP-HA construct in HEK293 cells is shown.

### **3.3 Immunoprecipitation of PKD3-FLAG and MP-GAP-FLAG**

#### **Optimization**

Immunoprecipitation experiments were initiated using cell lysates from two stable HEK293 cell lines, Stbl\_HEK293\_PKD3-FLAG and Stbl\_HEK293\_MP-GAP-FLAG, both of which were previously established using lentiviral constructs. These stable cell lines were generated to ensure consistent expression of the FLAG-tagged proteins PKD3 and MP-GAP. By integrating the constructs into the genome of HEK293 cells via lentiviral transduction, stable expression of these proteins was achieved, eliminating the variability associated with transient transfection. This approach ensures reliable experimental conditions for IP assays. Additionally, the stable cell lines facilitate long-term studies and allow for reproducibility in experiments aimed at investigating protein-protein interactions.

For the IP experiments, we used Anti-DYKDDDDK Affinity Resin Easy (GenScript, Cat#L00907), containing cross-linked agarose beads to monoclonal antibody against FLAG tag, to selectively capture FLAG-tagged proteins from the lysates. One critical step in optimizing the IP workflow was to identify a lysis buffer that would not only effectively lyse the cells, but also

preserve the protein-protein interactions required for downstream co-immunoprecipitation analysis. To this end, we tested different buffer formulations to achieve a balance between efficient cell lysis and preservation of protein integrity. Three different lysis buffers were tested to optimize the lysis conditions. Two of these buffers were prepared in-house, one containing Triton X-100 and the other NP-40, the specific compositions of which are described in the Materials and Methods section. The third was a commercially purchased IP lysis buffer formulated with NP-40 (see Table 7. Cell Lysis Buffer Composition, Chapter II). The IP experiments using these lysis buffers were performed according to the Anti-DYKDDDDK Affinity Resin Easy protocol. To evaluate the effectiveness of each buffer, three independent IP experiments were performed using the same amount of cell lysates, each containing approximately 120  $\mu\text{g}$  (corresponds to one well of a six-well plate, 80-90% cell confluency) of total protein derived from the Stbl\_HEK293\_PKD3-DYK cells. For each IP, the input, wash (the solution collected after the bead and lysate incubation step), and elution fractions were loaded onto an SDS-PAGE gel for Western blot analysis. This allowed for a direct comparison of the lysis efficiency and successful IP, defined by clear and specific isolation of the target protein, with minimal background noise and non-specific binding, as indicated by distinct bands in the elution fraction of the Western blot, together with efficient removal of unbound material in the wash as indicated by the absence of a band in those lanes as shown and described in Figure 15. Having identified the optimal lysis buffer for the IP of PKD3-FLAG, we tested whether the same conditions would give satisfactory results for MP-GAP-FLAG. The same IP conditions optimized for PKD3-FLAG were applied to MP-GAP-FLAG, using the anti-DYKDDDDK affinity resin and Pierce™ IP lysis buffer (buffer #2). Approximately 120  $\mu\text{g}$  of total protein from Stbl\_HEK293\_MP-GAP-DYK cell lysates was used for each IP. Following the same

protocol, we were able to successfully isolate MP-GAP-FLAG, as confirmed by a clear and distinct signal on the Western blot. However, in addition to the expected MP-GAP-FLAG band, two non-specific bands (around ~96 kDa and ~55 kDa) were detected in the elution fraction as shown in Figure 16. These same non-specific bands were also present in the elution fraction of the IP performed on non-transfected HEK293 cell lysates using the anti-DYKDDDDK affinity resin. While these non-specific bands did not interfere with the detection of MP-GAP-FLAG, their presence indicated a need for further refinement of the IP, which was further investigated later in the course of the project. (See 3.4.2 PKD3-FLAG and MP-GAP-HA Co-immunoprecipitation).

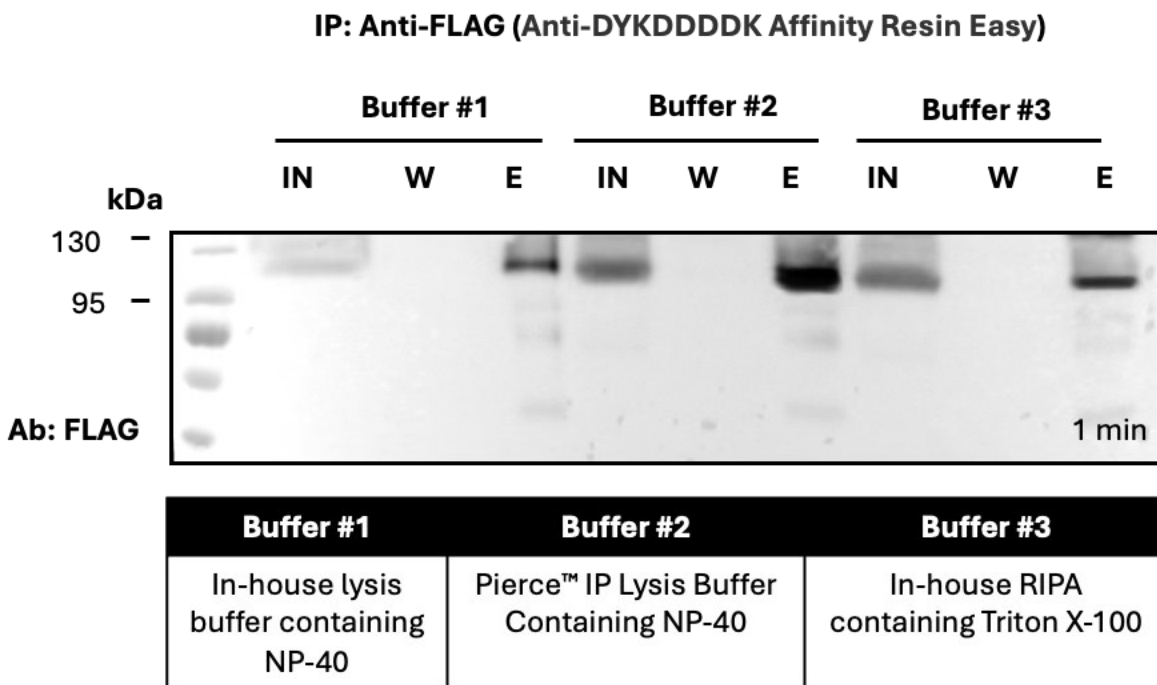


**Figure 15. Comparison of Lysis Buffers for Immunoprecipitation Using Anti-DYKDDDDK Affinity Resin**

The Western blot displays the input (IN), wash (W), and elution (E) samples from three separate IPs of PKD3-FLAG using stbl\_HEK293\_PKD3-FLAG cell lysates, each performed using different lysis buffers with the same initial amount of cell lysate. The results indicate that Buffers #2 and #3 performed better compared to Buffer #1, with clearer bands visible in the elution fractions, indicating successful capture of the target protein PKD3-FLAG. Buffer #2, Pierce™ IP Lysis Buffer, yielded the strongest bands in the elution samples, suggesting it provided the best conditions for efficient immunoprecipitation with this resin. Buffer #3, while effective, produced slightly weaker results compared to Buffer #2. Based on these findings, Buffer #2 was selected for continued use in subsequent experiments.

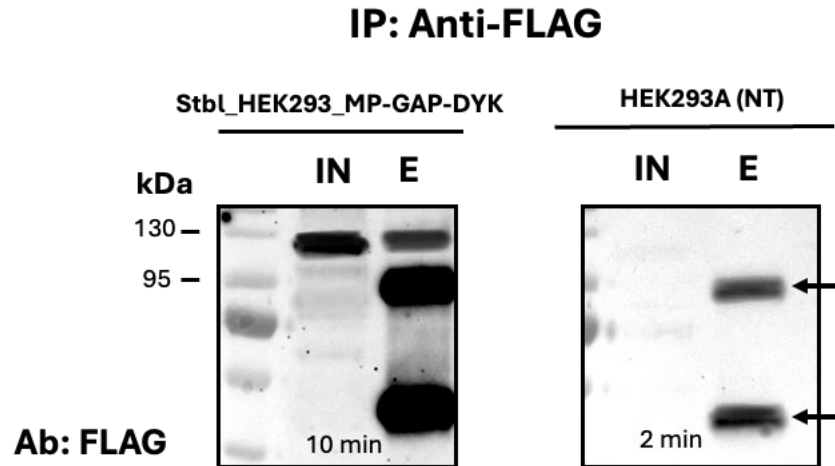


**Figure 16. MP-GAP-FLAG Immunoprecipitation**

The Western blot shows the IP of MP-GAP-FLAG using the optimized setup (anti-DYKDDDDK affinity resin and Pierce™ IP Lysis Buffer). It shows strong bands in both the input and elution fractions, confirming the successful isolation of MP-GAP-FLAG after 10 minutes of exposure. However, in the elution sample, two additional bands appeared. These bands are also present in the non-transfected control lysate marked by arrows.

## 3.4 Co-Immunoprecipitation

### 3.4.1 Co-IP positive control: TRIM47-Myc and PKD3-FLAG

To assess whether the optimized immunoprecipitation setup was effective in capturing protein-protein interactions, we used a positive control by testing the interaction between PKD3-FLAG and one recently established PKD3 binding partner, TRIM47. This interaction has been previously reported in HEK293 cells by Azuma, K. et al.2021, thus providing a suitable control for our co-immunoprecipitation conditions. We obtained a pcDNA3.1-TRIM47-Myc construct (GenScript, Clone ID: OHu05456, Accession Number: NM\_033452.3 ) containing a Myc tag. This construct was transiently transfected into Stb1-HEK293-PKD3-DYK cells to co-express both PKD3-FLAG and TRIM47-Myc in the same cellular environment. We then used the established IP setup with the anti-DYKDDDDK affinity resin, to co-immunoprecipitate TRIM47-Myc with PKD3-FLAG. The co-immunoprecipitation experiment to test the interaction between PKD3-FLAG and TRIM47-Myc was successful, as shown in

## IP: Anti-FLAG

Stbl\_HEK293\_PKD3-DYK

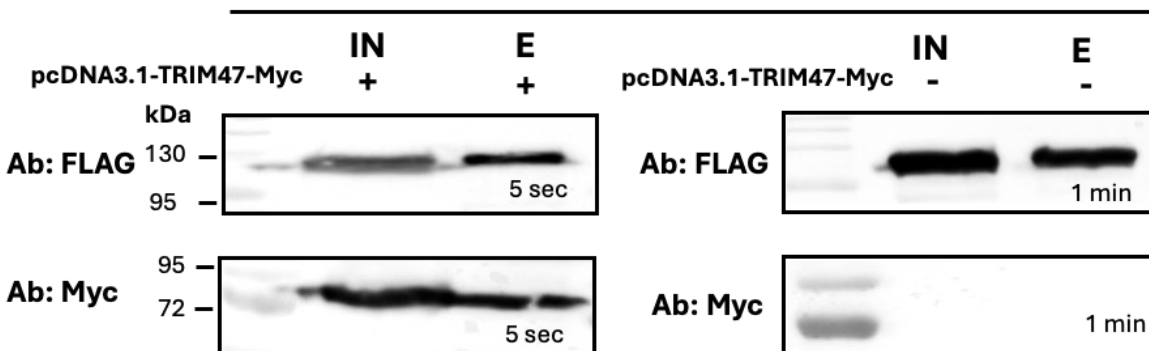
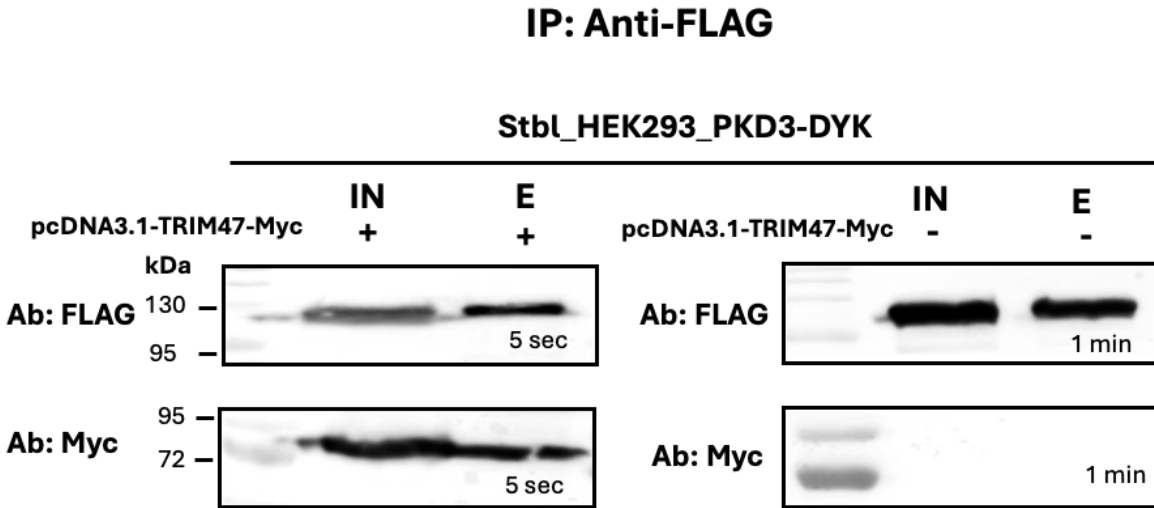


Figure 17. Western blot analysis confirmed the presence of both proteins in the expected fractions. Probing with an anti-FLAG antibody showed a strong PKD3-FLAG band in both input and elution samples, indicating efficient pull-down during immunoprecipitation. Similarly, probing with an anti-Myc antibody detected TRIM47-Myc in input and elution fractions, confirming its co-immunoprecipitation with PKD3-FLAG. This successful co-IP served as a positive control, validating the method for subsequent interaction studies with MP-GAP-FLAG.



**Figure 17. Successful Co-Immunoprecipitation of PKD3-FLAG and TRIM47-MYC as a Positive Control**

Western blot analysis showing the successful co-IP of PKD3-FLAG and TRIM47-Myc using Anti-DYKDDDDK Affinity Resin. Detection of PKD3-FLAG in both input (IN) and elution (E) fractions when the membrane was probed with anti-FLAG antibody, confirming efficient pull-down of PKD3-FLAG. Detection of TRIM47-Myc in the input (IN) and elution (E) fractions when the membrane was probed with anti-Myc antibody, indicating co-immunoprecipitation of TRIM47-Myc with PKD3-FLAG. Input lanes confirm protein expression, while elution lanes demonstrate successful capture of the interacting proteins. The negative control is immunoprecipitation from non-transfected Stbl-HEK293-PKD3-DYK cells, which shows bands when probed with anti-FLAG antibody but no detectable bands when probed with anti-Myc antibody, confirming the specificity of the Myc-tagged TRIM47 interaction.

### 3.4.2 PKD3-FLAG and MP-GAP-HA Co-immunoprecipitation

To investigate the potential interaction between PKD3-FLAG and MP-GAP-HA, three separate times using independently prepared cell lysates were performed. Each experiment was further repeated multiple times from the same lysate to confirm the consistency of the results. Stbl-HEK293-PKD3-DYK cells were transiently transfected with pcDNA3.1-MP-GAP-HA, co-expressing both PKD3-FLAG and MP-GAP-HA in these cells. Both input and elution samples were loaded onto SDS-PAGE gels for Western blot analysis. A negative control IP was performed in parallel using lysates from non-transfected Stbl-HEK293-PKD3-DYK cells. As shown in Figure 18, the input samples show the expression of both PKD3-FLAG and MP-GAP-HA, with signals corresponding to the expected molecular weights when probed with their respective antibodies (anti-FLAG and anti-HA). However, in the elution fractions, while PKD3-FLAG was consistently detected, no prominent signal at the expected molecular weight of MP-GAP-HA was observed when the membrane was probed with an anti-HA antibody. Instead, a faint signal was observed at this position after 5 minutes of exposure. Interestingly, this weak band was not observed in subsequent rounds of Co-IP experiments, suggesting that the initial observation was likely a result of background noise or transient, non-specific binding rather than a true interaction (see Figure 19). In addition, a strong, non-specific signal at approximately 55 kDa was present in the elution samples and was also detected in the negative control elution fraction. Following the appearance of this non-specific band, the next steps in the project focused on identifying the origin and eliminating the cause of the band.

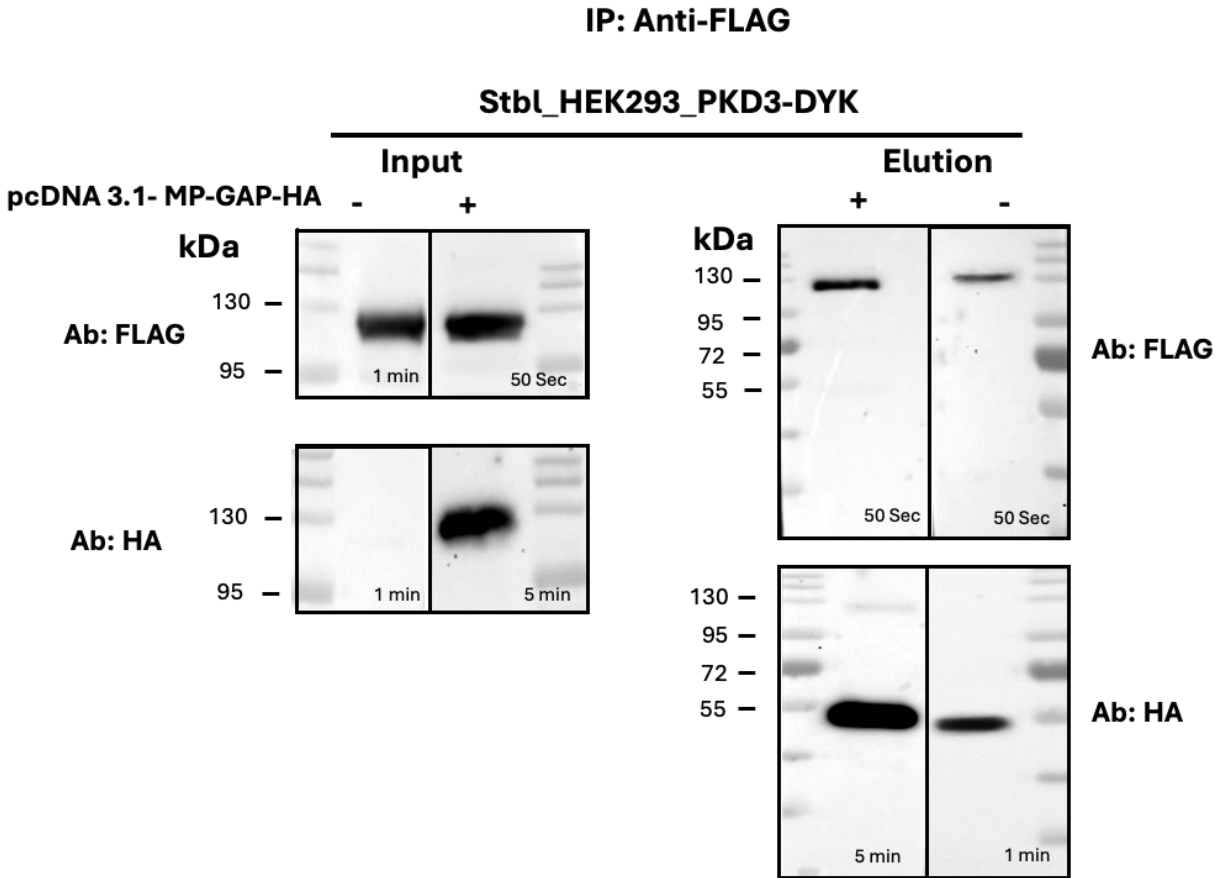


**Figure 18. PKD3-FLAG and MP-GAP-HA Co-Immunoprecipitation**

The Western blot panels present results from a co-IP experiment performed on stable HEK293 cells expressing PKD3-FLAG, which were transiently transfected with pcDNA3.1 MP-GAP-HA. The input and elution fractions from the Co-IP experiment were analyzed for the presence of MP-GAP-HA and PKD3-FLAG. The results show a significant nonspecific band in the elution samples (indicated by the arrow), which was also detected in the negative control (non-transfected cell lysates) later on. This large nonspecific band (~55 kDa) appeared consistently across different exposure times.

The next step in addressing the appearance of the prominent ~55 kDa band in the elution fractions was to investigate its origin. Given its molecular weight, this band could be the result of antibody cross-reactivity. Specifically, it was suggested that it could be due to the presence of antibodies in the elution sample itself, possibly from the resin, which could be recognized by the secondary antibody used in the Western blot detection procedure. One possible approach was to use a more stringent elution method or to modify the IP protocol to reduce antibody contamination in the elution. To this end, five independent immunoprecipitations were performed under different conditions. Two lysates from transfected Stbl-HEK293-PKD3-DYK cells with pcDNA3.1-MP-GAP-HA, two lysates from non-transfected Stbl-HEK293-PKD3-DYK cells, and one lysate from non-transfected HEK293 cells were included in the experiment. The aim was to determine whether the observed band was due to antibody cross-reactivity or other background signals.

Different elution methods were tested, including boiling the samples in SDS loading buffer and performing alkaline elution, to assess whether the elution technique had an effect on the presence or intensity of the non-specific 55 kDa band. In parallel, non-transfected cell lysates were processed under the same IP conditions to further investigate potential background signals or evidence for the source of the non-specific band. Western blot analysis of the eluate samples, as shown in Figure 19, panel B, revealed the presence of a strong non-specific band at approximately 55 kDa in all elution fractions when probed with the anti-HA antibody. This band was significantly more intense in the samples eluted by boiling in SDS loading buffer, which was the elution method initially used for the PKD3-FLAG and MP-GAP-HA co-IP experiments.

To minimize the possibility of this non-specific band masking any potential signal corresponding to MP-GAP-HA, the membrane was carefully cut in half before antibody incubation, separating

the upper and lower regions. This step was taken to ensure that any bands representing MP-GAP-HA in the higher molecular weight region would not be obscured by the strong non-specific signal in the lower region during imaging. Despite this precaution, no distinct band was detected in the molecular weight range expected for MP-GAP-HA, indicating that co-immunoprecipitation of MP-GAP-HA with PKD3-FLAG was not clearly observed under these experimental conditions. To definitively confirm that the non-specific ~55 kDa band observed in the elution fractions was due to secondary antibody binding to antibodies present in the elution, a final control Western blot was performed. Elution samples from previous IPs, all eluted by boiling in SDS loading buffer, were loaded on a SDS PAGE gel alongside a 'bead only' sample that was also boiled in the same buffer. This 'bead only' sample served as a control to assess whether antibodies from the IP setup itself were contributing to the observed non-specific band. In this experiment, the membrane was incubated and probed with the secondary antibody alone, without primary antibody incubation, to assess whether the secondary antibody was binding non-specifically to the antibodies eluted from the immunoprecipitation. The results as shown in Figure 20 indicated that the non-specific signal at ~55 kDa appeared in all the samples, including the 'bead only' control. This confirmed that the band was due to the secondary antibody binding to antibodies present in the elution samples, rather than being related to MP-GAP-HA or any other specific protein in the experiment.

Overall, The Co-IP experiments conducted to investigate a potential interaction between PKD3-FLAG and MP-GAP-HA did not provide conclusive evidence of such an interaction under the tested conditions. The presence of non-specific bands highlighted challenges in the Co-IP setup, emphasizing the need for further optimization or alternative approaches which will be discussed in the next chapter.

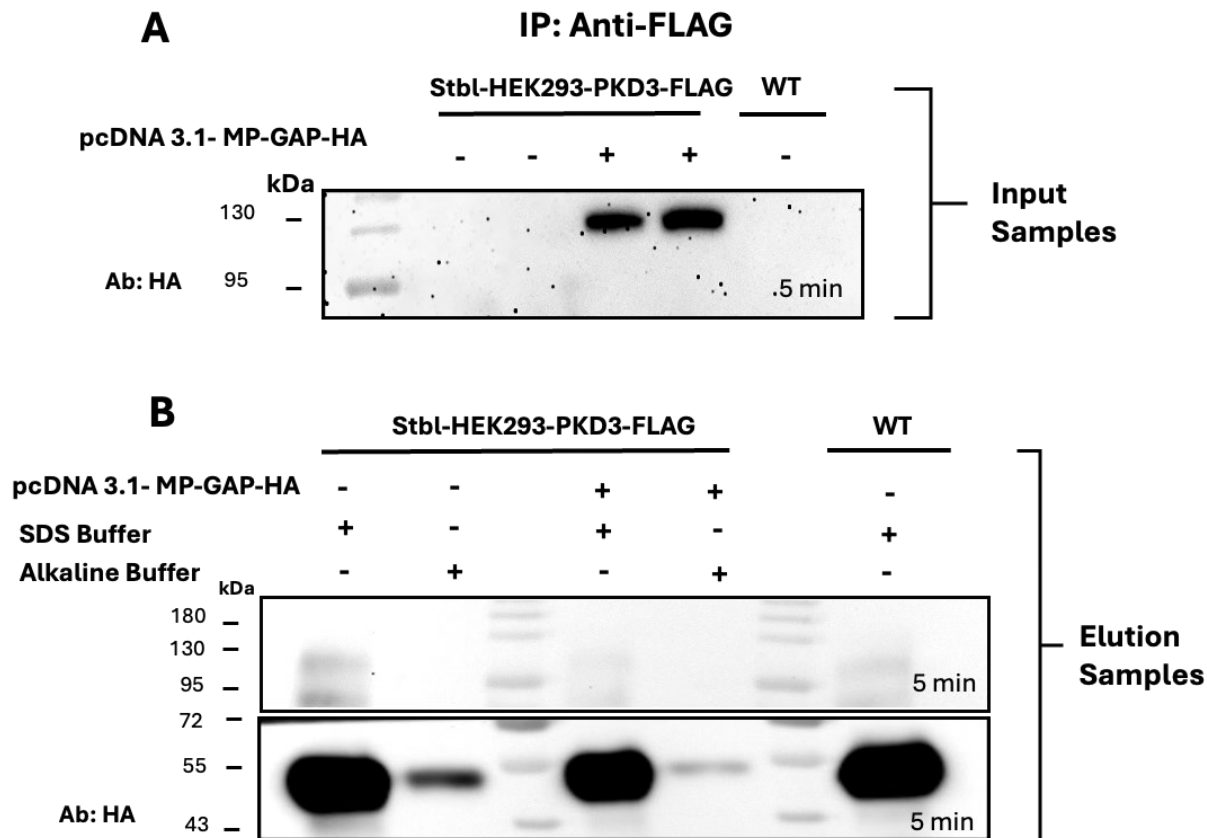


**Figure 19. Investigation of Nonspecific Bands Across Various Elution Methods in IP Experiments**

This figure shows the results of five independent IPs performed under different conditions to assess nonspecific binding across various elution methods. IPs were conducted on two lysates from non-transfected stable HEK293-PKD3-FLAG cells and two lysates from transiently transfected HEK293-PKD3-FLAG with pcDNA3.1-MP-GAP-HA cells, using either boiling with SDS buffer or alkaline elution. A control IP was also performed on wild-type HEK293 cells with SDS boiling to check for background noise. The membranes were cut in half to separately incubate with antibodies and image upper and lower sections, avoiding stronger bands from masking faint signals. Nonspecific bands were observed in all elution samples but were particularly intense with the SDS boiling method. Alkaline elution showed a reduced nonspecific signal.

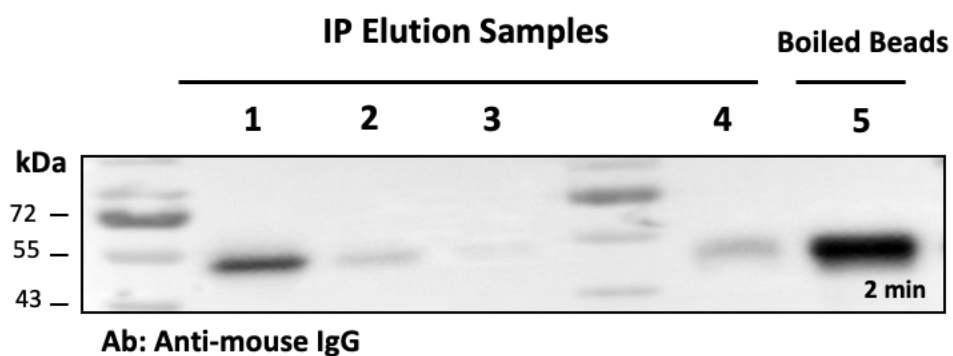


**Figure 20. Analyzing the Origin of the Non-specific Band**

To investigate the origin of the nonspecific band seen in previous Co-IPs, elution samples from previous Co-IPs and a sample of beads boiled with SDS-PAGE loading buffer were used in the western blot. The membrane was probed using only the secondary antibody to determine if the band resulted from the nonspecific binding of the secondary antibody. As shown in the blot, the same nonspecific band appeared across all samples.

## Chapter IV

### 4. Discussion

The primary objective of this project was to establish a Co-IP of the potential interaction between PKD3 and MP-GAP. During the study, several challenges arose that affected the progress of the experimental workflow. One obstacle was the low expression levels of the GST-tagged constructs used in this study, which limited their availability for subsequent analyses and required significant troubleshooting. In addition, significant cytotoxicity during the first transfections resulted in high cell death, complicating the workflow and requiring adjustments to the transfection conditions to improve cell viability. Also, background noise in the Co-IP assays, due to non-specific antibody binding obscured potential signals and complicated data interpretation. Despite overcoming many of these technical issues, the final Co-IP experiments could not provide evidence for an interaction between PKD3 and MP-GAP. However, the positive control confirmed the functionality of the basic Co-IP setup. The following sections will focus on exploring potential reasons for the lack of detectable interaction, suggesting solutions, and suggesting future directions for the continuation of this project.

#### 4.1 Potential Causes for Experimental Setbacks

##### 4.1.1 Exploring the Lack of MP-GAP-GST Expression and Differential Expression of FLAG-Tagged Constructs

During the course of this project, attempts were made to express PKD3 and MP-GAP as GST fusion proteins in CHO-K1 and HEK293 cells using constructs cloned in-house. Whilst PKD3-GST was detected by Western blot, MP-GAP-GST was undetectable, even though the construct was validated by restriction enzyme digestion to confirm correct insertion and orientation of the inserts, and further verified by sequencing to ensure that no mutations or frameshifts were present. The lack of a reasonable expression of MP-GAP-GST is likely due to one or a combination of factors, including protein instability, misfolding, and inefficient translation.

One major contributing factor could be the rapid degradation of MP-GAP by the ubiquitin-proteasome system, as supported by recent findings published in 2024 by Bagci et al. The hGID4 E3 ubiquitin ligase complex specifically targets ARHGAP11A (MP-GAP) for proteasomal degradation by binding and ubiquitinating it.<sup>61</sup> The study shows that depletion of GID4 or inhibition of its substrate binding pocket with PFI-7 stabilizes ARHGAP11A protein levels, indicating the crucial role of this pathway in its degradation. Furthermore, ARHGAP11A has a remarkably short half-life of under 4 hours, which can be the reason that complicates its detection and accumulation in experimental systems. Notably, the study demonstrated that the degradation mechanism not only regulates ARHGAP11A stability but also plays an essential role in cell migration by controlling its levels at the cell periphery, where it inactivates RhoA.<sup>61</sup>

While GST tagging often stabilizes proteins, it may instead cause improper folding of MP-GAP, leading to even greater susceptibility to degradation<sup>62</sup>. In contrast, FLAG-tagged MP-GAP, although expressed at lower levels than PKD3-FLAG, appeared to have more stable expression, possibly due to the smaller size of the FLAG tag, which allows for better folding and stability. The consistently lower expression of MP-GAP, regardless of the tag used, suggests that the protein itself may be inherently unstable or subject to rapid degradation within the cell.

Differences in transcriptional regulation or protein turnover rates between MP-GAP and PKD3 could also explain why PKD3 consistently shows higher expression levels.

Some beneficial approaches for this issue are to explore different expression conditions or consider alternative tags that may better stabilize MP-GAP, which was done in this project. Moreover, the use of more sensitive detection methods such as fluorescence-based techniques<sup>63</sup>, and mass spectrometry<sup>64</sup>, may help to detect lower levels of MP-GAP and determine the exact causes of the observed instability. In addition, since it was shown in recent publications that MP-GAP is rapidly degraded in cells, strategies such as inhibiting the hGID4 E3 ubiquitin ligase complex or using the PFI-7 inhibitor to block GID4's substrate binding pocket could stabilize its levels. However, these approaches are hypothetical and may have unintended effects on cellular pathways, requiring careful evaluation and validation.

#### 4.1.2 Background Noise and Antibody Binding

During the Co-IP experiments, one of the main problems encountered was significant background noise due to non-specific antibody binding. This consistent non-specific band of approximately ~55 kDa was observed in several independent experiments. The band, which appeared regardless of whether the target proteins were expressed or not, posed a challenge in interpreting the results. Further investigation revealed that this non-specific band was likely due to secondary antibody binding to eluted antibodies during the Co-IP process that had been covalently linked to the beads. In typical Co-IP setups, antibodies are immobilized on beads to capture the target protein. However, in some cases, the antibody used for this capture can be eluted along with the target protein during the elution step, resulting in the detection of the heavy (~50-55 kDa) and light (~25 kDa) chains of the antibody when probed with secondary antibodies

on a Western blot <sup>65</sup>. This background signal could obscure the detection of the proteins of interest, especially if the bands related to the proteins of interest are already weak.

To overcome this problem, gentler elution methods, such as low pH or competitive elution, can help prevent the release of antibody chains into the elution samples. Switching to directly labeled primary antibodies with HRP eliminates the need for secondary antibodies, which are a common source of background noise. This is because the secondary antibody, typically an anti-IgG, can interact with the eluted antibody chains present in the sample, leading to nonspecific signals. By avoiding the use of secondary antibodies, this approach minimizes such interactions and reduces background noise.

In this study, although the membrane was cut based on molecular weight to separate regions affected by the nonspecific band from those containing the target proteins, no prominent band appeared in the expected area, indicating the absence of detectable MP-GAP in the eluted sample. This absence does not necessarily confirm the protein's absence in the eluted sample but may indicate that its levels were below the detection threshold or masked by technical limitations in the assay which will be reviewed in the following sections.

## **4.2. Interpreting the Lack of Interaction in Co-IP: Implications and Future Directions**

Despite extensive efforts to optimize the experimental conditions, the Co-IP experiments performed during my thesis were not able to provide strong evidence for an interaction between

PKD3 and MP-GAP. Several potential factors could account for this negative result which will be discussed below.

#### 4.2.1 Low Protein Expression as a Negative Impact on the Co-IP

The relatively low expression of MP-GAP compared to PKD3 may have made it difficult to detect any interaction, even if it existed. Insufficient protein expression can severely limit the chances of detecting interactions in Co-IP experiments, where the abundance of both interacting partners needs to be adequate for stable complex formation<sup>66</sup>. However, it is noteworthy that a lower expression system may also have advantages, as it more closely mimics physiological conditions and reduces the likelihood of detecting artificial interactions that can arise from high overexpression levels.

To address the challenges associated with the low expression of MP-GAP, several approaches could potentially improve protein yield, though their effectiveness would need to be tested and validated. Cloning strategies such as codon optimization may enhance translation efficiency by aligning the codon usage of MP-GAP with the preferences of the host cell, potentially increasing protein production<sup>67,68</sup>. Additionally, using advanced cell lines specifically engineered for high protein production, such as HEK293-6E or CHO-K1-derived lines (such as ExpiCHO system by Gibco) with enhanced chaperone systems and optimized glycosylation pathways, could provide a more favorable environment for expressing MP-GAP<sup>69,70</sup>. Inducible expression systems in these cell lines could also help regulate protein levels, minimizing potential cytotoxic effects from overexpression. While these strategies appear promising, their ability to enhance MP-GAP

expression in this context remains uncertain and would require systematic testing to determine their feasibility and impact.

A reciprocal Co-IP, where both interacting proteins are tested as bait and prey in separate experiments, is considered a more comprehensive approach to detecting protein-protein interactions. In the timeline of this project, I was only able to perform the Co-IP by immobilizing PKD3, which is more abundantly expressed. However, attempting the reverse setup, immobilizing MP-GAP on the beads or performing the IP with beads targeting MP-GAP, might increase the likelihood of observing the interaction. This approach could help efficiently capture and concentrate the less abundant MP-GAP, minimizing its loss during washes and enhancing the detectability of any interaction. Exploring this reciprocal strategy would complement other optimization efforts and represent a more thorough method for confirming potential interactions between MP-GAP and PKD3.

#### 4.2.2. Influence of Post-Translational Modifications and Subcellular Localization

It is also possible that post-translational modifications, such as phosphorylation of PKD3, are required for its interaction with MP-GAP. If PKD3 needs to be activated by phosphorylation at specific stages of the cell cycle, this may explain the lack of detectable interaction under unsynchronized conditions. Subcellular localization may also have played a role, with the predicted interaction only occurring in a specific compartment of the cell at a certain stage, such as the cleavage furrow during cytokinesis.

To investigate these possibilities, complementary approaches have been employed in our lab alongside Co-IP assays. Fluorescence microscopy approaches such as live-cell imaging is used to

visualize the localization and interaction of PKD3 and MP-GAP in real-time. Techniques such as Förster Resonance Energy Transfer (FRET) can detect the close proximity of these proteins in living cells, providing insight into where and when these interactions occur during the cell cycle. FRET-based imaging, combined with fluorescent protein tagging (e.g., GFP or mCherry), allows for the monitoring of protein interactions in specific cellular locations and compartments, such as the cleavage furrow and the cytoskeleton, and in response to post-translational modifications such as phosphorylation. As these experiments are ongoing and conducted by other members of the research team, data from these approaches cannot be presented in this thesis.

#### 4.2.3 Weak or Transient Interactions

Another consideration is that the affinity of the interaction between PKD3 and MP-GAP may be too weak or transient to be captured under the Co-IP conditions used. Protein interactions can range from strong, stable complexes to weak, transient contacts that only occur under certain physiological conditions<sup>71</sup>. It is possible that the conditions used in this study, such as the choice of lysis buffer, salt concentrations, or incubation times, were not effective in stabilizing this interaction to capture such transient interactions, one effective approach is cross-linking, a technique that chemically stabilizes weak or short-lived protein-protein interactions by creating covalent bonds between interacting proteins. Cross-linking reagents are typically bifunctional or multifunctional molecules that contain reactive groups capable of targeting specific amino acid side chains. By using these reagents, interactions that occur transiently in the natural cellular environment can be “frozen” in place, providing a snapshot of the dynamic protein landscape at the moment of treatment. Cross-linking reagents such as formaldehyde and glutaraldehyde offer

straightforward applications. Formaldehyde targets primary amines and hydroxyl groups, effectively cross-linking closely associated proteins, while glutaraldehyde reacts with amines and is particularly useful for stabilizing complexes in preparation for imaging or structural studies.

<sup>72</sup>To enhance the temporal and spatial resolution of interaction studies, sulfo-SBED, a photoactivatable cross-linker, can be used. Upon UV activation, this reagent creates covalent bonds between proteins in close proximity and includes a biotin tag for downstream purification. This feature can be advantageous for isolating complexes like PKD3 and MP-GAP that might interact briefly during specific phases of the cell cycle like cytokinesis. In addition to cross-linking, different buffer conditions could be explored to favor weak interactions. For example, lower salt concentrations or the inclusion of specific stabilizing agents such as Ficoll in the lysis buffer may help to preserve the integrity of weaker protein complexes that might otherwise dissociate under standard conditions. <sup>73,74</sup>

Another alternative technique for detecting transient interactions is proximity-based labeling, such as BioID (Biotin Identification), TurboID or APEX (ascorbate peroxidase proximity labeling). These approaches rely on a promiscuous enzyme fused to one of the target proteins, which covalently labels all nearby proteins within a certain range. This labelling can capture interactions that occur transiently or in specific cellular microenvironments without requiring direct, long-lasting binding between proteins. After biotinylation, the labeled proteins can be affinity-purified and identified using mass spectrometry, providing a more sensitive approach to studying transient or context-specific interactions. <sup>75-77</sup>

#### 4.2.4 Indirect Interactions and Complex Formation

It is possible that the predicted interaction between PKD3 and MP-GAP is indirect and mediated by other proteins or cofactors that were not present in the experimental setup. Co-IP experiments rely on the physical binding between two proteins, but if the interaction is mediated by an intermediate protein, this would not be detected without the presence of the full protein complex. Future experiments could explore alternative approaches such as Tandem Affinity Purification (TAP) to identify potential mediators of the interaction.

TAP is a robust method designed to isolate protein complexes under near-physiological conditions, reducing the chance of disruption of indirect or weak interactions in experimental setups. This technique involves tagging one of the proteins of interest with a dual-affinity tag, such as a combination of Protein A and calmodulin-binding peptide or other tag pairs. These tags enable a sequential two-step purification process, where the protein of interest and its associated interactors are isolated and enriched, minimizing the loss of intermediate proteins.<sup>78</sup>

Once purified, the components of the protein complex can be identified using mass spectrometry, which would provide a comprehensive profile of co-purified proteins potentially mediating the PKD3-MP-GAP interaction. This approach would not only confirm the presence of intermediates but could also offer insights into the broader network of interactions involving PKD3 and MP-GAP.

### **4.3 Studying PKD3 in the Context of the Cell Cycle and Cytokinesis**

The cellular context in which these experiments were performed may also not reflect the physiological conditions required for PKD3 and MP-GAP to interact. Protein interactions can be highly context-dependent, influenced by cell state, post-translational modifications, or the

presence of specific signaling pathways that were not activated in the experimental cell system used here. <sup>79</sup>This is particularly relevant given that our hypothesis specifically analyzes PKD3 in the context of cell cycle regulation and cytokinesis progression.

#### 4.3.1 Synchronization of Cells and Time-course Analysis for Improved Detection

As the cells used in the Co-IP experiments were not synchronized and therefore not in the precise phase of the cell cycle where PKD3 and MP-GAP are most likely to interact, this may have significantly affected the likelihood of detecting an interaction. Synchronizing the cells to ensure they were in the correct phase may have provided a more suitable environment for these proteins to interact and increased the chances of observing a meaningful result.

In addition to cell synchronization, time-course experiments could be used to capture dynamic interactions by analyzing different time points post-transfection. In the context of this study, time-course experiments could provide insights into whether the PKD3-MP-GAP interaction occurs only during specific cellular events or time windows. Collecting cell lysates at intervals (e.g., every few hours after transfection) and performing Co-IP at each point would enable a detailed analysis of interaction dynamics. This approach is particularly useful when combined with synchronized cell populations, ensuring that the timing of sample collection aligns with relevant cell cycle phases, such as mitosis or cytokinesis, where these proteins are most likely to interact. Furthermore, monitoring protein expression levels at each time point using Western blotting ensures that interactions are assessed during periods of sufficient protein availability. Complementary techniques, such as flow cytometry for cell cycle staging or live-cell imaging, can provide additional context, helping to correlate observed interactions with cellular events. If

the interaction is transient or mediated by other proteins, time-course experiments may also reveal indirect effects, such as changes in the abundance or post-translational modifications of associated proteins.<sup>80</sup>

#### **4.4 Future Directions**

All of the previous sections highlight the broader challenge of studying PKD3 in the context of cell cycle regulation and cytokinesis. Notwithstanding these challenges, the study of PKD3 function remains crucial because of its potential involvement in important cellular events such as cytokinesis, which have wider implications in pathological conditions such as cancer.

In addition to the approaches mentioned above to improve the analysis of the PKD3-MP-GAP interaction, a valuable next step would be to use proteomic studies to gain a more comprehensive understanding of the broader PKD3 interaction network. A valuable approach to further elucidate the role of PKD3 would be to apply mass spectrometry (MS)-based proteomics to analyze PKD3's interacting partners during specific cell cycle phases. A study by D'Avino et al. (2019) provides a framework for this type of investigation, in which they examined the midbody interactome using a high-throughput MS-based approach<sup>81</sup>. By synchronizing cells into the appropriate phase of the cell cycle and using PKD3 as bait, similar pull-down experiments could be performed to identify top interacting partners. By using mass spectrometry to analyze pull-down results, it may be possible to narrow down the list of potential PKD3 interacting partners, which would provide valuable insights into its role during cytokinesis.

However, this type of study has its own challenges. High throughput approaches such as MS generate large data sets that require parallel validation and rigorous *in vivo* studies to confirm the physiological relevance of the identified interactions. These novel studies, while promising, need

to be complemented by functional assays in living cells to verify the role of these interactions and their involvement in the cell cycle. In addition, the regulatory mechanisms of PKD3, such as post-translational modifications and its activity in different cellular contexts, need to be carefully considered to fully understand its role during specific stages of the cell cycle.

## **4.5 Implications for Cancer Research and Therapeutic Strategies**

Despite the challenges of functional studies, these studies are vital, particularly in cancer research, where understanding the intricate mechanisms of cell cycle regulation can pave the way for new therapeutic strategies. Proteins like PKD3, involved in cytokinesis and cell division, are critical targets for cancer therapies due to their central role in cellular proliferation. Advances in targeting kinases involved in cell cycle regulation, such as cyclin-dependent kinases (CDKs), Aurora kinases, and Polo-like kinases (PLKs), have already revolutionized cancer treatment by disrupting critical checkpoints in cell division. Cyclin-dependent kinases (CDKs) are central regulators of the cell cycle, controlling transitions through phases like G1/S and G2/M. CDK inhibitors, such as palbociclib, ribociclib, and abemaciclib, have been successfully used to treat hormone receptor-positive breast cancers by arresting tumor cells in the G1 phase. Similarly, Aurora kinases, which are essential for chromosome alignment and segregation during mitosis, have become promising targets. Inhibitors like alisertib aim to exploit their roles in mitotic spindle assembly to induce cancer cell death. PLKs, especially PLK1, are another class of mitotic kinases that regulate centrosome maturation and cytokinesis. PLK1 inhibitors, such as volasertib, have shown potential in preclinical and clinical trials for various malignancies. These kinase inhibitors demonstrate the therapeutic power of targeting cell cycle dysregulation but are

not without limitations. Resistance mechanisms, including compensatory pathway activation, and off-target effects remain significant challenges. Furthermore, tumor heterogeneity and the adaptive nature of cancer cells often limit the long-term efficacy of these therapies. Addressing these issues requires a more comprehensive understanding of kinase interactions and functions in the context of specific cellular environments<sup>82-84</sup>.

A deeper exploration of PKD3's role in cytokinesis and its interaction network could reveal new opportunities to target cell cycle-related processes, offering innovative strategies to overcome therapeutic resistance. Such insights might extend beyond oncology, impacting conditions like fibrotic diseases, where aberrant cell proliferation drives pathology, or developmental disorders tied to cell cycle dysregulation. Ultimately, the ability to precisely map PKD3's interactions within the cellular environment is not just a step toward unraveling fundamental biological processes, it represents a pathway to innovation in disease treatment.

## REFERENCES

1. Lee MJ, Yaffe MB. Protein regulation in signal transduction. *Cold Spring Harb Perspect Biol.* 2016;8(6). doi:10.1101/cshperspect.a005918
2. Ardito F, Giuliani M, Perrone D, Troiano G, Muzio L Lo. The crucial role of protein phosphorylation in cell signaling and its use as targeted therapy (Review). *Int J Mol Med.* 2017;40(2):271-280. doi:10.3892/ijmm.2017.3036
3. Nishi H, Shaytan A, Panchenko AR. Physicochemical mechanisms of protein regulation by phosphorylation. *Front Genet.* 2014;5(AUG). doi:10.3389/fgene.2014.00270
4. Cheng HC, Qi RZ, Paudel H, Zhu HJ. Regulation and function of protein kinases and phosphatases. *Enzyme Res.* 2011;2011(1). doi:10.4061/2011/794089
5. Bill CA, Vines CM. Phospholipase C. In: *Advances in Experimental Medicine and Biology.* Vol 1131. Springer New York LLC; 2020:215-242. doi:10.1007/978-3-030-12457-1\_9
6. Black AR, Black JD. Protein kinase C signaling and cell cycle regulation. *Front Immunol.* 2012;3(JAN). doi:10.3389/fimmu.2012.00423
7. Takai Y, Kishimoto A, Iwasa Y, Kawahara Y, Mori T, Nishizuka Y. Calcium-dependent activation of a multifunctional protein kinase by membrane phospholipids. *Journal of Biological Chemistry.* 1979;254(10):3692-3695. doi:10.1016/s0021-9258(18)50638-4
8. Huang KP. *The Mechanism of Protein Kinase C Activation.*; 1989.
9. Steinberg SF. Structural basis of protein kinase C isoform function. *Physiol Rev.* 2008;88(4):1341-1378. doi:10.1152/physrev.00034.2007
10. Wang H, Kazanietz MG. Chimaerins, novel non-protein kinase C phorbol ester receptors, associate with Tmp21-I (p23): Evidence for a novel anchoring mechanism involving the chimaerin

- C1 domain. *Journal of Biological Chemistry*. 2002;277(6):4541-4550.  
doi:10.1074/jbc.M107150200
11. Yang CF, Kazanietz MG. Divergence and complexities in DAG signaling: Looking beyond PKC. *Trends Pharmacol Sci*. 2003;24(11):602-608. doi:10.1016/j.tips.2003.09.003
  12. Kazanietz MG. *Novel "Nonkinase" Phorbol Ester Receptors: The C1 Domain Connection*. Vol 61.; 2002.  
<http://molpharm.aspetjournals.org><http://molpharm.aspetjournals.org/content/61/5/1265.full.pdf>
  13. Chang L, Karin M. *Mammalian MAP Kinase Signalling Cascades*. Vol 410.; 2001.  
[www.nature.com](http://www.nature.com)
  14. Starr TK, Jameson SC, Hogquist KA. Positive and negative selection of T cells. *Annu Rev Immunol*. 2003;21:139-176. doi:10.1146/annurev.immunol.21.120601.141107
  15. Yang Y, Calakos N. Munc13-1 is required for presynaptic long-term potentiation. *Journal of Neuroscience*. 2011;31(33):12053-12057. doi:10.1523/JNEUROSCI.2276-11.2011
  16. Cai J, Abramovici H, Gee SH, Topham MK. Diacylglycerol kinases as sources of phosphatidic acid. *Biochim Biophys Acta Mol Cell Biol Lipids*. 2009;1791(9):942-948.  
doi:10.1016/j.bbalip.2009.02.010
  17. Storz P, Döppler H, Toker A. Protein Kinase D Mediates Mitochondrion-to-Nucleus Signaling and Detoxification from Mitochondrial Reactive Oxygen Species. *Mol Cell Biol*. 2005;25(19):8520-8530. doi:10.1128/mcb.25.19.8520-8530.2005
  18. Fu Y, Rubin CS. Protein kinase D: Coupling extracellular stimuli to the regulation of cell physiology. *EMBO Rep*. 2011;12(8):785-796. doi:10.1038/embor.2011.139

19. Johannes FJ, Prestle J, Eis S, Oberhagemann P, Pfizenmaier K. PKCu is a novel, atypical member of the protein kinase C family. *Journal of Biological Chemistry*. 1994;269(8):6140-6148.  
doi:10.1016/s0021-9258(17)37580-4
20. Hayashi A, Seki N, Hattori A, Kozuma S, Saito T. *Short Sequence-Paper PKCX, a New Member of the Protein Kinase C Family, Composes a Fourth Subfamily with PKCW 1.*
21. Sturany S, Van Lin J, Müller F, et al. Molecular cloning and characterization of the human protein kinase D2: A novel member of the protein kinase D family of serine threonine kinases. *Journal of Biological Chemistry*. 2001;276(5):3310-3318. doi:10.1074/jbc.M008719200
22. Rozengurt E, Rey O, Waldron RT. Protein kinase D signaling. *Journal of Biological Chemistry*. 2005;280(14):13205-13208. doi:10.1074/jbc.R500002200
23. Reinhardt R, Truebestein L, Schmidt HA, Leonard TA. It Takes Two to Tango: Activation of Protein Kinase D by Dimerization. *BioEssays*. 2020;42(4):1900222.  
doi:<https://doi.org/10.1002/bies.201900222>
24. Roy A, Ye J, Deng F, Wang QJ. Protein kinase D signaling in cancer: A friend or foe? *Biochimica et Biophysica Acta (BBA) - Reviews on Cancer*. 2017;1868(1):283-294.  
doi:10.1016/J.BBCAN.2017.05.008
25. Zugaza JL, Waldron RT, Sinnott-Smith J, Rozengurt E. *Bombesin, Vasopressin, Endothelin, Bradykinin, and Platelet-Derived Growth Factor Rapidly Activate Protein Kinase D through a Protein Kinase C-Dependent Signal Transduction Pathway\**; 1997. <http://www.jbc.org>
26. Elsner DJ, Siess KM, Gossenreiter T, Hartl M, Leonard TA. A ubiquitin-like domain controls protein kinase D dimerization and activation by trans-autophosphorylation. *Journal of Biological Chemistry*. 2019;294(39):14422-14441. doi:10.1074/JBC.RA119.008713

27. Reinhardt R, Truebestein L, Schmidt HA, Leonard TA. It Takes Two to Tango: Activation of Protein Kinase D by Dimerization. *BioEssays*. 2020;42(4):1900222. doi:<https://doi.org/10.1002/bies.201900222>
28. Rozengurt E. Protein kinase D signaling: Multiple biological functions in health and disease. *Physiology*. 2011;26(1):23-33. doi:10.1152/physiol.00037.2010
29. Roy A, Veroli MV, Prasad S, Wang QJ. Protein kinase D2 modulates cell cycle by stabilizing aurora a kinase at centrosomes. *Molecular Cancer Research*. 2018;16(11):1785-1797. doi:10.1158/1541-7786.MCR-18-0641
30. Rozengurt E, Rey O, Waldron RT. Protein kinase D signaling. *J Biol Chem*. 2005;280(14):13205-13208. doi:10.1074/JBC.R500002200
31. Prestle J, Pfizenmaier K, Brenner J, Johannes FJ. Protein kinase C mu is located at the Golgi compartment. *J Cell Biol*. 1996;134(6):1401. doi:10.1083/JCB.134.6.1401
32. Baron CL, Malhotra V. Role of Diacylglycerol in PKD Recruitment to the TGN and Protein Transport to the Plasma Membrane. *Science (1979)*. 2002;295(5553):325-328. doi:10.1126/science.1066759
33. Bossard C, Bresson D, Polishchuk RS, Malhotra V. Dimeric PKD regulates membrane fission to form transport carriers at the TGN. *Journal of Cell Biology*. 2007;179(6):1123-1131. doi:10.1083/jcb.200703166
34. Fugmann T, Hausser A, Schöffler P, Schmid S, Pfizenmaier K, Olayioye MA. Regulation of secretory transport by protein kinase D-mediated phosphorylation of the ceramide transfer protein. *Journal of Cell Biology*. 2007;178(1):15-22. doi:10.1083/jcb.200612017
35. Rozengurt E. Mitogenic signaling pathways induced by G protein-coupled receptors. *J Cell Physiol*. 2007;213(3):589-602. doi:<https://doi.org/10.1002/jcp.21246>

36. Sinnett-Smith J, Jacamo R, Kui R, et al. Protein Kinase D Mediates Mitogenic Signaling by Gq-coupled Receptors through Protein Kinase C-independent Regulation of Activation Loop Ser744 and Ser748 Phosphorylation. *Journal of Biological Chemistry*. 2009;284(20):13434-13445. doi:10.1074/JBC.M806554200
37. Sinnett-Smith J, Zhukova E, Hsieh N, Jiang X, Rozengurt E. Protein Kinase D Potentiates DNA Synthesis Induced by Gq-coupled Receptors by Increasing the Duration of ERK Signaling in Swiss 3T3 Cells. *Journal of Biological Chemistry*. 2004;279(16):16883-16893. doi:10.1074/JBC.M313225200
38. Wong C, Jin ZG. Protein kinase C-dependent protein kinase D activation modulates ERK signal pathway and endothelial cell proliferation by vascular endothelial growth factor. *Journal of Biological Chemistry*. 2005;280(39):33262-33269. doi:10.1074/jbc.M503198200
39. Chang HH, Wang W, Bong SJ, et al. Protein kinase D-dependent phosphorylation and nuclear export of histone deacetylase 5 mediates vascular endothelial growth factor-induced gene expression and angiogenesis. *Journal of Biological Chemistry*. 2008;283(21):14590-14599. doi:10.1074/jbc.M800264200
40. Johannessen M, Delghandi MP, Rykx A, et al. Protein kinase D induces transcription through direct phosphorylation of the cAMP-response element-binding protein. *Journal of Biological Chemistry*. 2007;282(20):14777-14787. doi:10.1074/jbc.M610669200
41. Rey O, Yuan J, Young SH, Rozengurt E. Protein Kinase C $\gamma$ /Protein Kinase D $\delta$  Nuclear Localization, Catalytic Activation, and Intracellular Redistribution in Response to G Protein-coupled Receptor Agonists. *Journal of Biological Chemistry*. 2003;278(26):23773-23785. doi:10.1074/JBC.M300226200
42. Storz P, Toker A. Protein kinase D mediates a stress-induced NF- $\kappa$ B activation and survival pathway. *EMBO J*. 2003;22(1):109-120. doi:https://doi.org/10.1093/emboj/cdg009

43. Morgan MJ, Liu ZG. Crosstalk of reactive oxygen species and NF- $\kappa$ B signaling. *Cell Res.* 2011;21(1):103-115. doi:10.1038/cr.2010.178
44. Sánchez-Ruiloba L, Cabrera-Poch N, Rodríguez-Martínez M, et al. Protein kinase D intracellular localization and activity control kinase D-interacting substrate of 220-kDa traffic through a postsynaptic density-95/discs large/zonula occludens-1-binding motif. *J Biol Chem.* 2006;281(27):18888-18900. doi:10.1074/JBC.M603044200
45. Matthews SA, Iglesias T, Rozengurt E, Cantrell D. Spatial and temporal regulation of protein kinase D (PKD). *EMBO J.* 2000;19(12):2935-2945-2945. doi:https://doi.org/10.1093/emboj/19.12.2935
46. Rey O, Yuan J, Rozengurt E. Intracellular redistribution of protein kinase D2 in response to G-protein-coupled receptor agonists. *Biochem Biophys Res Commun.* 2003;302(4):817-824. doi:10.1016/S0006-291X(03)00269-9
47. Rey O, Yuan J, Young SH, Rozengurt E. Protein kinase C  $\alpha$ /protein kinase D3 nuclear localization, catalytic activation, and intracellular redistribution in response to G protein-coupled receptor agonists. *J Biol Chem.* 2003;278(26):23773-23785. doi:10.1074/JBC.M300226200
48. Liu Y, Song H, Zhou Y, et al. The oncogenic role of protein kinase D3 in cancer. *J Cancer.* 2021;12(3):735. doi:10.7150/JCA.50899
49. Liu Y, Song H, Yu S, et al. Protein Kinase D3 promotes the cell proliferation by activating the ERK1/c-MYC axis in breast cancer. *J Cell Mol Med.* 2020;24(3):2135. doi:10.1111/JCMM.14772
50. Azuma K, Ikeda K, Suzuki T, Aogi K, Horie-Inoue K, Inoue S. TRIM47 activates NF- $\kappa$ B signaling via PKC- $\epsilon$ /PKD3 stabilization and contributes to endocrine therapy resistance in breast cancer. doi:10.1073/pnas.2100784118/-/DCSupplemental

51. Zhang T, Braun U, Leitges M. Cell Cycle PKD3 deficiency causes alterations in microtubule dynamics during the cell cycle. Published online 2016. doi:10.1080/15384101.2016.1188237
52. Saurin AT, Brownlow N, Parker PJ. Protein kinase C epsilon in cell division: Control of abscission. *Cell Cycle*. 2009;8(4):549-555. doi:10.4161/cc.8.4.7653
53. Saurin AT, Durgan J, Cameron AJ, Faisal A, Marber MS, Parker PJ. The regulated assembly of a PKCε complex controls the completion of cytokinesis. *Nat Cell Biol*. 2008;10(8):891-901. doi:10.1038/ncb1749
54. Chen J, Deng F, Singh S V., Wang QJ. Protein kinase D3 (PKD3) contributes to prostate cancer cell growth and survival through a PKCε/PKD3 pathway downstream of Akt and ERK 1/2. *Cancer Res*. 2008;68(10):3844-3853. doi:10.1158/0008-5472.CAN-07-5156
55. Basant A, Glotzer M. Spatiotemporal Regulation of RhoA during Cytokinesis. *Current Biology*. 2018;28(9):R570-R580. doi:10.1016/j.cub.2018.03.045
56. Basant A, Glotzer M. Spatiotemporal Regulation of RhoA during Cytokinesis. *Current Biology*. 2018;28(9):R570-R580. doi:10.1016/j.cub.2018.03.045
57. Prokopenko SN, Brumby A, O'keefe L, et al. *A Putative Exchange Factor for Rho1 GTPase Is Required for Initiation of Cytokinesis in Drosophila.*; 1999. www.genesdev.org
58. Loria A, Longhini KM, Glotzer M. The RhoGAP domain of CYK-4 Has an essential role in RhoA activation. *Current Biology*. 2012;22(3):213-219. doi:10.1016/j.cub.2011.12.019
59. Zanin E, Desai A, Poser I, et al. A conserved RhoGAP limits M phase contractility and coordinates with microtubule asters to confine RhoA during Cytokinesis. *Dev Cell*. 2013;26(5):496-510. doi:10.1016/j.devcel.2013.08.005

60. Kagawa Y, Matsumoto S, Kamioka Y, et al. Cell cycle-dependent Rho GTPase activity dynamically regulates cancer cell motility and invasion in vivo. *PLoS One*. 2013;8(12). doi:10.1371/journal.pone.0083629
61. Bagci H, Winkler M, Grädel B, et al. The hGID<sup>GID4</sup> E3 ubiquitin ligase complex targets ARHGAP11A to regulate cell migration. *Life Sci Alliance*. 2024;7(12):e202403046. doi:10.26508/lsa.202403046
62. Thermo Fisher Scientific. GST-tagged Proteins – Production and Purification.
63. Fuchs ACD. Specific, sensitive and quantitative protein detection by in-gel fluorescence. *Nat Commun*. 2023;14(1). doi:10.1038/s41467-023-38147-8
64. Burgess MW, Keshishian H, Mani DR, Gillette MA, Carr SA. Simplified and Efficient Quantification of Low-abundance Proteins at Very High Multiplex via Targeted Mass Spectrometry\*. *Molecular & Cellular Proteomics*. 2014;13(4):1137-1149. doi:https://doi.org/10.1074/mcp.M113.034660
65. Antrobus R, Borner GHH. Improved elution conditions for native co-immunoprecipitation. *PLoS One*. 2011;6(3). doi:10.1371/journal.pone.0018218
66. Free RB, Hazelwood LA, Sibley DR. Identifying novel protein-protein interactions using co-immunoprecipitation and mass spectroscopy. *Curr Protoc Neurosci*. 2009;(SUPPL. 46). doi:10.1002/0471142301.ns0528s46
67. Quax TEF, Claassens NJ, Söll D, van der Oost J. Codon Bias as a Means to Fine-Tune Gene Expression. *Mol Cell*. 2015;59(2):149-161. doi:10.1016/j.molcel.2015.05.035
68. Gustafsson C, Minshull J, Govindarajan S, Ness J, Villalobos A, Welch M. Engineering genes for predictable protein expression. *Protein Expr Purif*. 2012;83(1):37-46. doi:10.1016/J.PEP.2012.02.013

69. Torres M, Dickson AJ. Combined gene and environmental engineering offers a synergetic strategy to enhance r-protein production in Chinese hamster ovary cells. *Biotechnol Bioeng.* 2022;119(2):550-565. doi:<https://doi.org/10.1002/bit.28000>
70. Tan E, Chin CSH, Lim ZFS, Ng SK. HEK293 Cell Line as a Platform to Produce Recombinant Proteins and Viral Vectors. *Front Bioeng Biotechnol.* 2021;9. doi:10.3389/fbioe.2021.796991
71. Byrum S, Smart SK, Larson S, Tackett AJ. Analysis of stable and transient protein-protein interactions. *Methods in Molecular Biology.* 2012;833:143-152. doi:10.1007/978-1-61779-477-3\_10
72. Tang X, Bruce JE. Chemical cross-linking for protein-protein interaction studies. *Methods Mol Biol.* 2009;492:283-293. doi:10.1007/978-1-59745-493-3\_17
73. Brudar S, Hribar-Lee B. Effect of buffer on protein stability in aqueous solutions: A simple protein aggregation model. *Journal of Physical Chemistry B.* 2021;125(10):2504-2512. doi:10.1021/acs.jpcc.0c10339
74. Budayeva HG, Cristea IM. A mass spectrometry view of stable and transient protein interactions. *Adv Exp Med Biol.* 2014;806:263-282. doi:10.1007/978-3-319-06068-2\_11
75. Roux KJ, Kim DI, Raida M, Burke B. A promiscuous biotin ligase fusion protein identifies proximal and interacting proteins in mammalian cells. *Journal of Cell Biology.* 2012;196(6):801-810. doi:10.1083/jcb.201112098
76. Branon TC, Bosch JA, Sanchez AD, et al. Efficient proximity labeling in living cells and organisms with TurboID. *Nat Biotechnol.* 2018;36(9):880-898. doi:10.1038/nbt.4201
77. Kalocsay M. APEX peroxidase-catalyzed proximity labeling and multiplexed quantitative proteomics. In: *Methods in Molecular Biology.* Vol 2008. Humana Press Inc.; 2019:41-55. doi:10.1007/978-1-4939-9537-0\_4

78. Puig O, Caspary F, Rigaut G, et al. The Tandem Affinity Purification (TAP) Method: A General Procedure of Protein Complex Purification. *Methods*. 2001;24(3):218-229.  
doi:10.1006/METH.2001.1183
79. Fuxreiter M. Context-dependent, fuzzy protein interactions: Towards sequence-based insights. *Curr Opin Struct Biol*. 2024;87. doi:10.1016/j.sbi.2024.102834
80. Tang X, Wang J, Liu B, Li M, Chen G, Pan Y. A comparison of the functional modules identified from time course and static PPI network data. *BMC Bioinformatics*. 2011;12. doi:10.1186/1471-2105-12-339
81. Capalbo L, Bassi ZI, Geymonat M, et al. The midbody interactome reveals unexpected roles for PP1 phosphatases in cytokinesis. *Nat Commun*. 2019;10(1). doi:10.1038/s41467-019-12507-9
82. Suski JM, Braun M, Strmiska V, Sicinski P. Targeting cell-cycle machinery in cancer. *Cancer Cell*. 2021;39(6):759-778. doi:10.1016/j.ccell.2021.03.010
83. Kannaiyan R, Mahadevan D. A comprehensive review of protein kinase inhibitors for cancer therapy. *Expert Rev Anticancer Ther*. 2018;18(12):1249-1270.  
doi:10.1080/14737140.2018.1527688
84. Zhang M, Zhang L, Hei R, et al. *CDK Inhibitors in Cancer Therapy, an Overview of Recent Development*. Vol 11.; 2021. www.ajcr.us/